Pan-genome analysis identifies intersecting roles for *Pseudomonas* specialized metabolites in potato pathogen inhibition

Francesca L. Stefanato[1], Christine Trippel[1], Simon Uszkoreit[1], Laura Ferrafiat[1], Lucia Grenga[1], Ruth Dickens[1], Nathan Kelly[1], Alexander D. H. Kingdon[1], Liana Ambrosetti[1], Kim C. Findlay[2], Jitender Cheema[3], Martin Trick[3], Govind Chandra[1], Graham Tomalin[4], Jacob G. Malone[1,5*] and Andrew W. Truman[1*]

1. Department of Molecular Microbiology, John Innes Centre, Norwich, NR4 7UH, United Kingdom
2. Department of Cell and Developmental Biology, John Innes Centre, Norwich, NR4 7UH, United Kingdom
3. Department of Computational and Systems Biology, John Innes Centre, Norwich, NR4 7UH, United Kingdom
4. VCS Potatoes, 2 Burnt Cottages, Badingham Road, Framlingham, Suffolk, IP13 9HX, United Kingdom
5. School of Biological Sciences, University of East Anglia, Norwich, NR4 7TU, United Kingdom

***Corresponding authors**
andrew.truman@jic.ac.uk; jacob.malone@jic.ac.uk

Abstract

Agricultural soil harbors a diverse microbiome that can form beneficial relationships with plants, including the inhibition of plant pathogens. *Pseudomonas* are one of the most abundant bacterial genera in the soil and rhizosphere and play important roles in promoting plant growth and preventing disease. However, the genetic determinants of this beneficial activity are only partially understood, especially in relation to specialized metabolite production. Here, we genetically and phenotypically characterize the *Pseudomonas fluorescens* population in commercial potato field soils and identify strong correlations between specialized metabolite biosynthetic pathways and antagonism of the potato pathogens *Streptomyces scabies* and *Phytophthora infestans*. Genetic and chemical analyses identified hydrogen cyanide and cyclic lipopeptides as key specialized metabolites associated with *S. scabies* inhibition. We show that a single potato field contains a hugely diverse and dynamic population of *Pseudomonas* bacteria, whose capacity to produce specialized metabolites is shaped both by plant colonization and defined environmental inputs.

Introduction

Plant pathogenic microorganisms are responsible for major crop losses worldwide and represent a substantial threat to food security. Potato scab is a one of the main diseases affecting potato quality (1, 2), and presents a significant economic burden to farmers around the world. The Gram-positive bacterium *Streptomyces scabies*, which is the causal organism of potato scab, is ubiquitous and presents a threat in almost all soils (3). Properly managed irrigation is a reasonably effective control measure for potato scab. However, scab outbreaks still regularly occur in irrigated soil, and with increasing pressures on water use it is clear that alternative approaches to the control of scab are needed. An attractive potential alternative involves the exploitation of soil microorganisms that suppress or kill plant pathogens, known as biocontrol agents (4, 5).

Many soil-dwelling *Pseudomonas* species form beneficial relationships with plants, positively affecting nutrition and health (6-8) and exhibiting potent antagonistic behavior towards pathogenic microorganisms (9-12). *Pseudomonas* influence the plant environment using a diverse range of secondary metabolites (13-15) and secreted proteins (16, 17). As such, *Pseudomonas* sp. have been identified as key biocontrol organisms in numerous plant-microbe systems (18), and these bacteria have potential applications as agricultural biocontrol agents and biofertilizers (19, 20). Many soil pseudomonads belong to the *P. fluorescens* group, which consists of over 50 sub-species and exhibits huge phenotypic and genetic diversity (7, 21-23), with a core genome of about 1,300 genes and a pan-genome of over 30,000 genes (24). These bacteria use a variety of mechanisms to colonize the plant rhizosphere (25), communicate with plants (8), and suppress a range of plant pathogens (9), including bacteria (6), fungi (26) and insects (27), although a single strain is unlikely to have all of these attributes. Secondary metabolites are critical to many of these ecological functions, and the secondary metabolome of the pseudomonads is one of the richest and best characterized of any bacterial genus (13-15).

Various studies have associated pseudomonads with potato scab suppression. A significant increase in the abundance of *Pseudomonas* taxa has been observed for irrigated fields, correlating with reduced levels of potato scab (28). Naturally scab-suppressive soils have also been shown to contain a greater proportion of *Pseudomonas* when compared to scab-conducive soils (29, 30) and phenazine production by *P. fluorescens* can contribute to scab control in greenhouse experiments(20). Differences between soil microbial populations that enable effective pathogen suppression are routinely assessed using metagenomic tools (29, 31). However, the heterogeneity of the *P. fluorescens* group limits the usefulness of these

methods for observing changes at the species or even the genus level. To effectively determine the relationship between the soil *Pseudomonas* population and disease suppression, it is important to accurately survey genotypic and phenotypic variability at the level of individual isolates, and to determine how this variation is linked to agriculturally relevant environmental changes (32).

To investigate the genetic bases for *S. scabies* inhibition by *P. fluorescens* and to assess whether the scab-suppressive effects of irrigation derive from increased populations of biocontrol genotypes in the soil or on the plant, we focused on the *Pseudomonas* population from a potato field susceptible to potato scab. We first employed a phenotype-genotype correlation analysis across *P. fluorescens* strains isolated from a single potato field. We hypothesized that an unbiased correlation analysis would identify genetic loci and biosynthetic gene clusters that may be overlooked by screening for bioactive small molecules or by focusing on the biosynthetic repertoire of a limited number of strains. Here, we correlated phylogeny, phenotypes, secondary metabolism and accessory genome loci, then investigated the importance of strong correlations by genetic manipulation of selected wild isolates. In total, 432 *Pseudomonas* strains were phenotyped (with 69 whole-genome sequenced). This approach also enabled us to answer a number of ancillary questions: how diverse is the *P. fluorescens* population from a single field location? Do the phenotypes associated with a *P. fluorescens* strain correlate with its biosynthetic capacity? What does irrigation do to both the population structure of the *P. fluorescens* group and to the wider bacterial community? Using this approach, we show that irrigation induces profound and repeatable changes in the microbiome, both on a global level and within the *P. fluorescens* species group. We identify the *P. fluorescens* genes and gene clusters that are required for potato pathogen suppression *in vitro*. Finally, we use these data to explain the relationship between irrigation, pathogen suppression, and population-level shifts within the plant-associated *P. fluorescens* population.

Results

Irrigation induces a significant change in the soil microbiome

The ability of irrigation to protect root vegetables against *S. scabies* infection is agriculturally important and widespread, but poorly understood. It is likely that the irrigated soil microbiota plays a role in mediating scab suppression, but how this occurs is unclear. We therefore assessed the impact of irrigation on the total bacterial population of a commercial potato field in the United Kingdom. Multiple soil samples were taken from two sites (A1 and B1) within this field, immediately prior to potato planting in January. Following potato planting, one site was irrigated as normal (site A), while the second was protected from irrigation (site B). Tuber-associated soil was sampled from both sites in May (A2 and B2) when tubers were just forming,

and the plants were most susceptible to *S. scabies* infection. Total genomic DNA was then extracted from replicate samples of each site after each sampling event, and 16S rRNA amplicon sequencing was used to examine the bacterial population in each of these sites (Figure 1, Figure S1).

We used voom (33) with a false discovery rate (FDR) of 0.05 to assess population changes across the four sampling sites. In total, changes were observed for 26 bacterial orders (Figure 1A), with the most significant changes observed between January and May regardless of irrigation. This partially reflects an increase in bacterial orders that have previously been associated with the potato root microbiome (34, 35), including *Rhizobiales*, *Sphingomonadales* and *Flavobacteriales*. Significant population changes (FDR<0.05) were also observed for 8 bacterial orders between the irrigated (A2) and non-irrigated (B2) sites (Figure 1B and 1C), including a larger proportion of *Pseudomonadales* bacteria in the irrigated site. In contrast, despite the potential for microbial heterogeneity across the fertilized field prior to planting, no significant changes were observed between pre-planting sites A1 and B1.

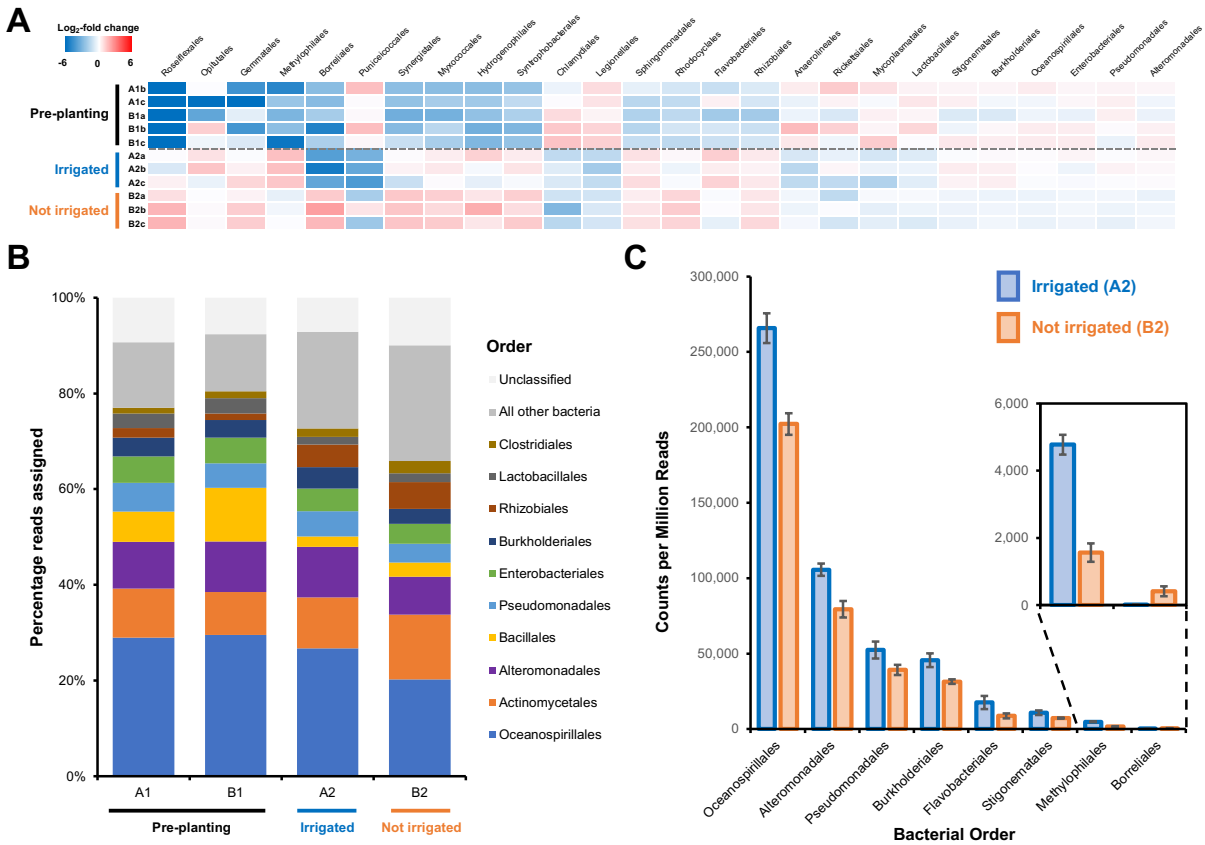

Figure 1 Effect of irrigation on the microbial population of a potato field. (A) The 26 bacterial orders whose populations were determined to significantly differ across one or more sampling sites using voom with a false discovery rate of 0.05. Data is shown as a heatmap of the $\log_2$-fold change with respect to the overall average counts per million for a given order. Sample A1a was omitted from the analysis due

132 to possible contamination leading to an atypical bacterial population (Figure S1). (B) Overall average
133 population of each sample site showing the 10 most abundant bacterial orders across all sites. (C) The
134 eight bacterial orders whose populations were determined to significantly differ between irrigated and
135 non-irrigated sites, represented as counts per million reads. Error bars represent the standard deviation
136 of triplicate data.
137

138 **Phenotypic, phylogenetic and genomic analysis of the *P. fluorescens* field population**

139 Taxonomic identifications using 16S rRNA amplicon analysis showed order-level changes to
140 the field microbiome between sites (Figure S1) but were unable to accurately capture diversity
141 within genera or species groups. Therefore, biologically relevant variation within the populations
142 of genetically diverse species groups such as *P. fluorescens* is potentially overlooked. To
143 investigate the diversity of the fluorescent pseudomonad population, we isolated 240 individual
144 *Pseudomonas* strains from our pre- and post-irrigation field sites (Supporting Dataset 1). These
145 strains were screened for multiple phenotypes including motility, protease production,
146 fluorescence (siderophore production) and on-plate suppression of *S. scabies* using a cross-
147 streak assay (Figures S2 and S3). Each phenotype was scored on an ordinal scale between 0
148 (no phenotype observed) and 3 (strong phenotype). The cross-streak assay provided a rapid
149 read-out of bacterial antagonism for both contact-dependent and diffusible mechanisms of
150 growth inhibition. On-plate suppression of *S. scabies* was a surprisingly rare trait, with 79% of
151 *Pseudomonas* isolates out-competed by *S. scabies* in this assay. To determine whether this
152 suppressive activity correlated with specific genetic loci, 69 isolates were selected for whole
153 genome sequencing, where almost half (32 strains) exhibited on-plate suppression of *S. scabies*
154 and the remaining strains represented a diverse selection (based on phenotypic variation and
155 16S rRNA sequencing) of non-suppressive strains. We hypothesized that a comparative
156 analysis of a similar number of genomes from suppressive and non-suppressive strains would
157 identify those biosynthetic gene clusters (BGCs) that play important roles in suppressive activity.
158

159 The phylogeny of the 69 sequenced strains was analyzed alongside various model
160 pseudomonads, including representatives of the eight phylogenomic *P. fluorescens* groups
161 defined by Garrido-Sanz *et al.* (24). Our sequenced strain collection spans much of this
162 characterized global phylogenetic diversity and contains representatives of at least five of the
163 eight *P. fluorescens* phylogenomic groups (24), as well as strains belonging to the *P. putida* and
164 *P. syringae* groups (Figure S4). This genetic heterogeneity was also reflected in the diverse
165 secondary metabolome of these strains, as predicted by a detailed analysis of the BGCs
166 encoded in their genomes. Each genome was subjected to antiSMASH analysis (36), which
167 was further refined by extensive manual annotation to improve the accuracy of predicted
168 pathway products. This second annotation step was particularly important for BGCs that are

169 atypically distributed across two distinct genomic loci (e.g. viscosin and pyoverdine). Our
170 analysis was further expanded to include BGCs not identified by antiSMASH 4.0, including
171 BGCs for hydrogen cyanide (HCN) (37), microcin B17-like pathways (38) and the auxin indole-
172 3-acetic acid (IAA). This was achieved by searching the genomes with a personally curated set
173 of known *Pseudomonas* gene clusters using MultiGeneBlast (39) (see Supplementary
174 Information for further details). This manual annotation provided a level of resolution superior to
175 that provided by automated cluster-searching algorithms alone and provided confidence that
176 the majority of natural product biosynthetic potential had been identified. Within a given pathway
177 type (e.g. non-ribosomal peptide synthetases, NRPSs), likely pathway products were assigned
178 where possible (e.g. cyclic lipopeptides, CLPs) or assigned a code when a conserved
179 uncharacterised BGC was identified (e.g. NRPS1). All BGCs were mapped to strain phylogeny
180 (Figure 2).
181

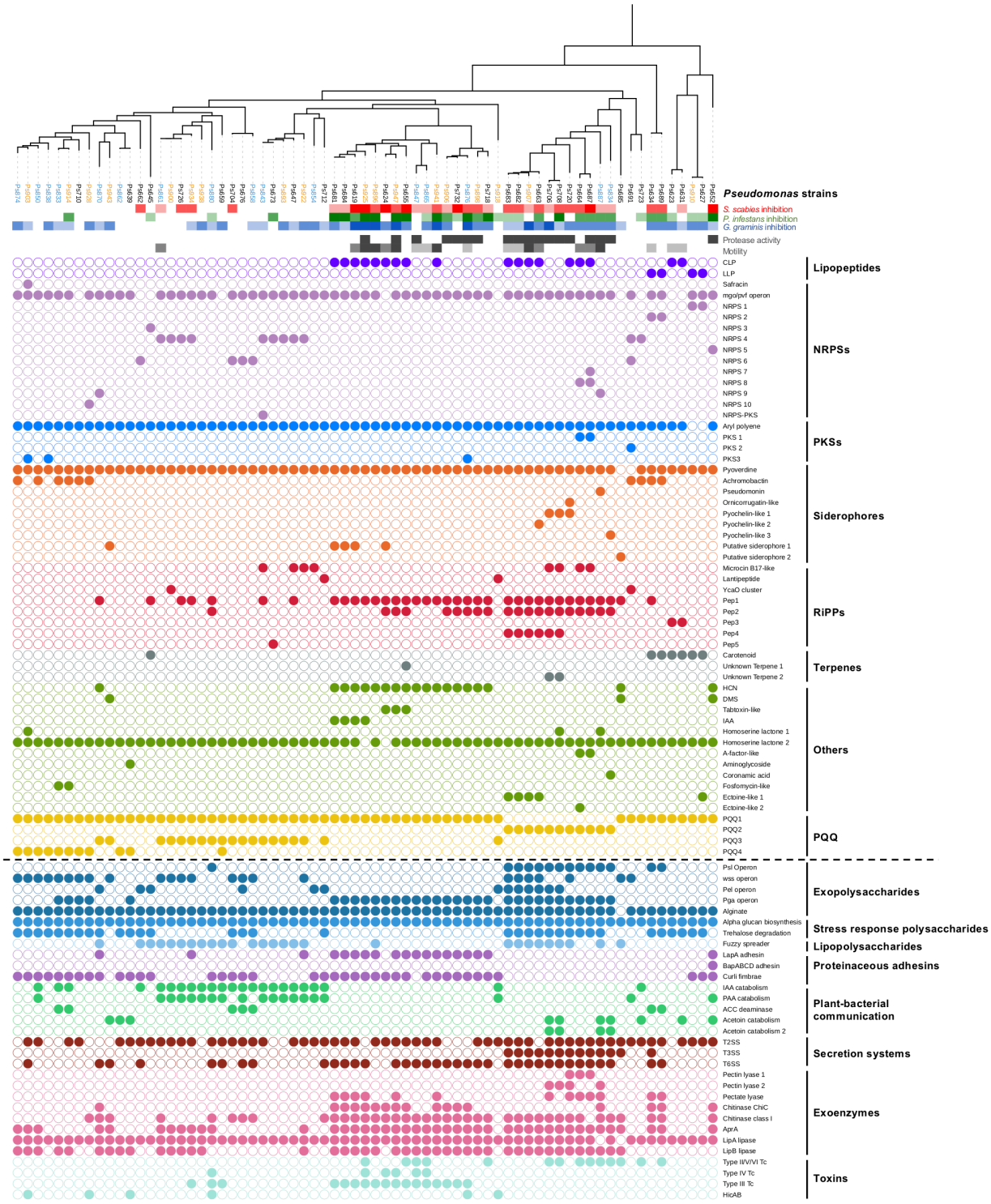

Figure 2 Comparison of phylogeny, *S. scabies* suppression (red colour scales), *P. infestans* suppression (green colour scale), *Gaeumannomyces graminis* pv. *tritici* (take-all) suppression (blue colour scale), phenotypes (grey colour scales), natural product biosynthetic gene clusters (filled circles = presence of a gene or gene cluster) and the accessory genome (separated from BGCs by a dotted line). In the phylogenetic tree of *Pseudomonas* strains, blue strains were collected from irrigated plots while orange strains were collected from unirrigated plots. All other strains were collected from the pre-irrigation plots.

191 As expected, almost every strain had the genetic potential to make the fluorescent siderophore
192 pyoverdine. Furthermore, other BGCs were commonly found across the sequenced strains,
193 including BGCs predicted to make CLPs (40), arylpolyenes (41) and HCN (37). The unexpected
194 isolation of a few *P. syringae* strains meant that some linear lipopeptide (LLP) BGCs were also
195 found (42). Numerous siderophore BGCs were identified, including pathways predicted to make
196 achromobactin (43), ornicorrugatin (44), pyochelin-like molecules and a pseudomonin-like
197 molecule (45). Curiously, all pyochelin-like BGCs feature one more NRPS module than the
198 characterised pathway (46) (Figure S5). A variety of polyketide synthase (PKS), terpene and
199 NRPS BGCs with no characterised homologues were also identified (Figure 2). Furthermore,
200 eight strains had BGCs with high homology to the microcin B17 pathway (38, 47), two strains
201 had BGCs predicted to make fosfomycin-like antibiotics (48) (Figure S6), and two strains had
202 lantipeptide BGCs (49). One strain contained a BGC predicted to produce the anti-tumour
203 molecule safracin (13), one strain encoded a putative carbapenem BGC (50) and one strain
204 encoded an aminoglycoside-like BGC (51) (Figure S6). Each of these natural product classes
205 is predicted to have potent biological activity and some are rarely found in pseudomonads.
206
207 In addition to these potentially antibacterial and cytotoxic compounds, four strains contain BGCs
208 predicted to produce the plant auxin IAA and one strain was predicted to produce coronamic
209 acid (52). While 23 genomes contained genes for IAA catabolism, these strains do not overlap
210 with the four IAA producers. All 69 strains had BGCs for the production of the electron-transport
211 cofactor pyrroloquinoline quinone (53) (PQQ), reported to function as a plant growth
212 promoter(54). Curiously, four different versions of the PQQ BGC were identified that differed by
213 the precise genes present in each BGC (Figure S7), while a subset of strains contained two
214 PQQ BGCs (Figure 2). Surprisingly, gene clusters for a variety of well characterised
215 *Pseudomonas* secondary metabolites were not observed. For example, no strains were
216 predicted to make phenazines, pyrrolnitrin or 2,4-diacylphloroglucinol (13). In total, 571 gene
217 clusters were identified that could be sub-divided into 55 gene cluster families (Figure 2).
218
219 The large *P. fluorescens* pan-genome means that the species group possesses a highly diverse
220 array of non-essential accessory genes and gene clusters. These are often critical to the lifestyle
221 of a given strain, and can include motility determinants, proteases, secretion systems,
222 polysaccharides, toxins and metabolite catabolism pathways. We therefore searched our strains
223 for accessory genome loci using MultiGeneBlast (details in Supporting Information), which
224 revealed a high degree of genomic diversity across strains. Both secondary metabolism BGCs
225 and accessory genome loci were mapped to strain phylogeny (Figure 2), which indicated that
226 for some loci (e.g. the *psl* operon, auxin catabolism, HCN biosynthesis) there is a close, but not
227 absolute, relationship between phylogeny and the presence of a gene cluster.

228

229 **Correlation analysis identifies potential genetic determinants of *S. scabies* inhibition**

230 We hypothesised that genes associated with suppression of *S. scabies* could be identified by a
231 correlation analysis between *S. scabies* cross-streak inhibition and the presence of gene cluster
232 families or accessory genes. We therefore calculated Pearson correlation coefficients for each
233 gene cluster with *S. scabies* inhibition (Figure S8). The top 10 positively correlating genotypes
234 and phenotypes that were highly overrepresented in suppressive strains (Figure 3) comprised
235 four gene cluster families (Pep1, CLP, Pep2 and HCN) (Figure S9), four accessory genome loci
236 (chitinase ChiC, protease AprA, chitinase class 1 and the Pga operon) and two phenotypes
237 (motility and secreted protease production). The production of HCN and/or CLPs by
238 *Pseudomonas* strains have been previously associated with the suppression of various plant
239 pathogens including fungi (26, 55) and oomycetes (19, 56), and can also contribute to insect
240 killing (27, 57), but have not been linked to the suppression of bacteria. In contrast, a variety of
241 genotypes associated with plant-microbe interactions were moderately negatively correlated
242 with suppression ($\rho < -0.3$), including gene clusters for PQQ biosynthesis and catabolism of the
243 plant auxins IAA and phenylacetic acid (PAA) (Figure 3A).

244

245 Interestingly, while certain BGC loci (e.g. CLP) positively correlated with both suppression and
246 motility, this relationship was not seen for every locus (e.g. HCN correlates with suppression
247 but is less strongly correlated with motility). Correlation does not equate to causation, especially
248 considering the significant evolutionary association seen for some gene clusters (Figure 3C).
249 The importance of correlating BGCs to *S. scabies* suppression was therefore investigated
250 experimentally using a genetically tractable subset of suppressive isolates.

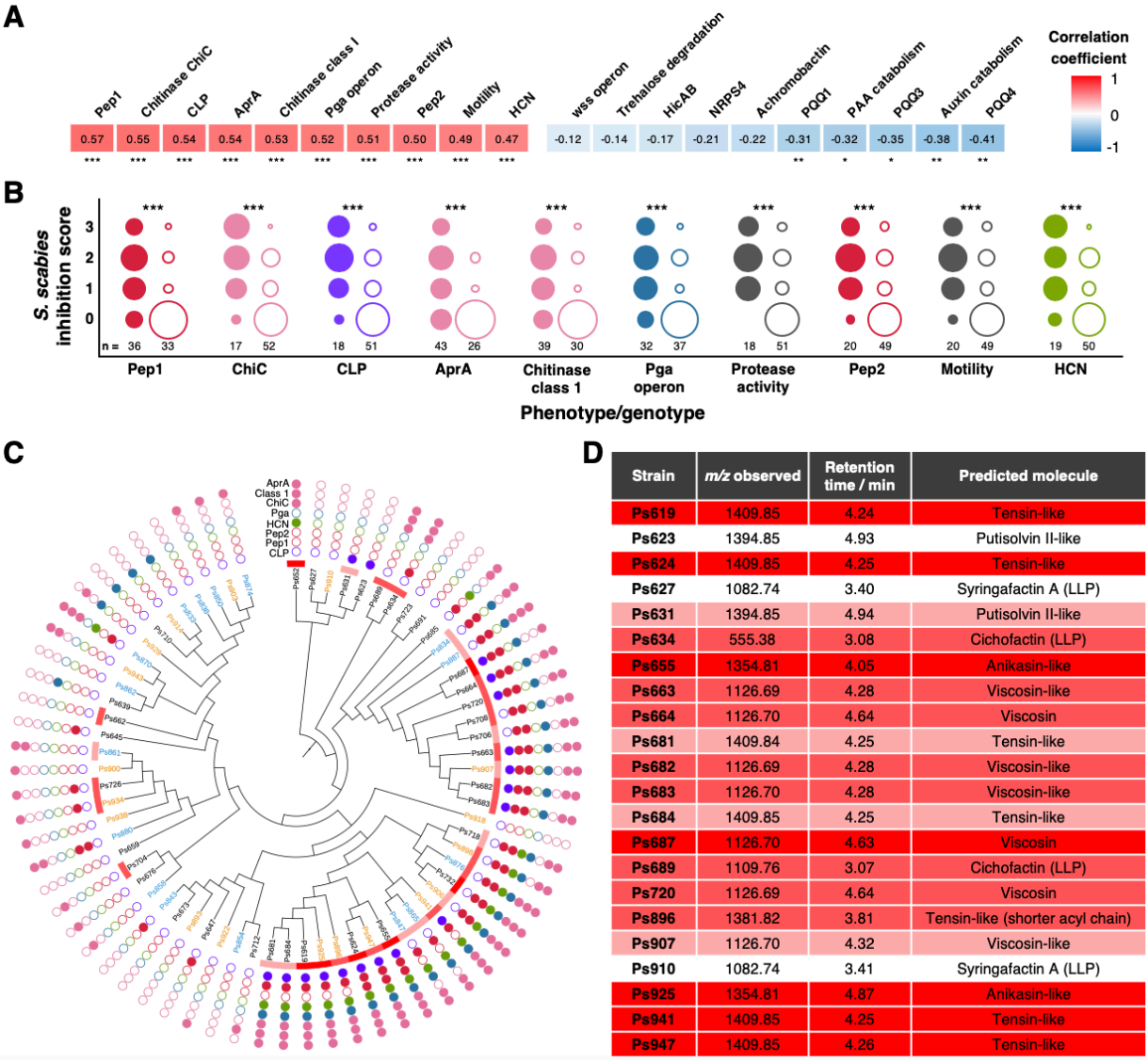

Strain	*m/z* observed	Retention time / min	Predicted molecule
Ps619	1409.85	4.24	Tensin-like
Ps623	1394.85	4.93	Putisolvin II-like
Ps624	1409.85	4.25	Tensin-like
Ps627	1082.74	3.40	Syringafactin A (LLP)
Ps631	1394.85	4.94	Putisolvin II-like
Ps634	555.38	3.08	Cichofactin (LLP)
Ps655	1354.81	4.05	Anikasin-like
Ps663	1126.69	4.28	Viscosin-like
Ps664	1126.70	4.64	Viscosin
Ps681	1409.84	4.25	Tensin-like
Ps682	1126.69	4.28	Viscosin-like
Ps683	1126.70	4.28	Viscosin-like
Ps684	1409.85	4.25	Tensin-like
Ps687	1126.70	4.63	Viscosin
Ps689	1109.76	3.07	Cichofactin (LLP)
Ps720	1126.69	4.64	Viscosin
Ps896	1381.82	3.81	Tensin-like (shorter acyl chain)
Ps907	1126.70	4.32	Viscosin-like
Ps910	1082.74	3.41	Syringafactin A (LLP)
Ps925	1354.81	4.87	Anikasin-like
Ps941	1409.85	4.25	Tensin-like
Ps947	1409.85	4.26	Tensin-like

Figure 3 Correlation of BGCs and accessory genome loci with *S. scabies* inhibition. (A) Heatmap showing the 10 genotypes and phenotypes that correlated most strongly (positively and negatively) with on-plate suppression of *S. scabies*. Stars represent the statistical significance of a correlation using a Chi-squared test ($p<0.05$ = *, $p<0.01$ = **, $p<0.001$ = ***). (B) Distributions of *S. scabies* suppressive activity for top 10 positive correlations. Circles are stacked from no (0) to high (3) inhibition, where filled and empty circles represent strains with and without a given genotype, respectively. The number of strains (total = 69) in each class is listed, and the area of a circle specifies the proportion of strains with given suppressive activity. (C) Top correlating genotypes mapped to strain phylogeny. (D) Production of lipopeptides by strains containing lipopeptide BGCs. Colour-coding reflects level of *S. scabies* inhibition by each strain (LLP = linear lipopeptide; all others are CLPs).

Production and role of CLPs in suppression of *S. scabies*

The strong positive correlation between putative CLP gene clusters and *S. scabies* suppression prompted us to investigate whether CLPs play a role in suppressive activity. *Pseudomonas* CLPs have previously been associated with a wide array of functions, including fungal growth

267 inhibition, plant colonisation and promotion of swarming motility (40, 58), although there are no
268 reports of *Pseudomonas* CLPs functioning as inhibitors of streptomycete growth. However, prior
269 work has shown that surfactin, a CLP from *Bacillus subtilis,* inhibits *Streptomyces coelicolor*
270 aerial hyphae development (59), while iturin A, a CLP from *Bacillus* sp. sunhua, inhibits *S.*
271 *scabies* development (60). Prior to investigating the role of the *Pseudomonas* CLPs, we sought
272 to confirm their identity in each strain. CLPs are produced by modular NRPSs, which enabled
273 a rational prediction of the products of these pathways (14) (Figure 3D).
274
275 To validate our preliminary sequence-based annotations, strains were assessed for their ability
276 to make CLPs using liquid chromatography – tandem mass spectrometry (LC-MS^2). In every
277 strain that contained a CLP gene cluster, a molecule with an expected mass and MS^2
278 fragmentation pattern was identified (Figure 3D, Figures S10-S16). This showed that *P.*
279 *fluorescens* strains from a single field have the collective capacity to make viscosin (*m/z*
280 1126.69, identical retention time to a viscosin standard), a viscosin isomer (*m/z* 1126.69,
281 different retention time to viscosin standard) (Figures S10 and S11), as well as compounds with
282 gene clusters, exact masses and MS^2 fragmentation consistent with tensin (*m/z* 1409.85, Figure
283 S12) (61), anikasin (*m/z* 1354.81, Figure S13) (62), and putisolvin II (*m/z* 1394.85, Figure S14)
284 (63). In addition, an array of related metabolites were observed that differed by 14 or 28 Da,
285 which is characteristic of different lipid chain lengths. This analysis also proved that the linear
286 lipopeptides syringafactin A (*m/z* 1082.74) and cichofactin (*m/z* 555.38, $[M+2H]^{2+}$) were made
287 by strains harbouring BGCs predicted to make these phytotoxins (13, 64) (Figures S15 and
288 S16). This diversity was mapped using mass spectral networking with the Global Natural
289 Product Social Molecular Networking (GNPS) server (65, 66). This networked metabolite data
290 was used to visualize the inhibitory capacity of the strains that produce a specific metabolite
291 (Figure 4). As anticipated from the genotypic data, CLPs were strongly associated with strains
292 that inhibit *S. scabies* (red nodes in Figure 4 indicate molecules from inhibitory strains).
293

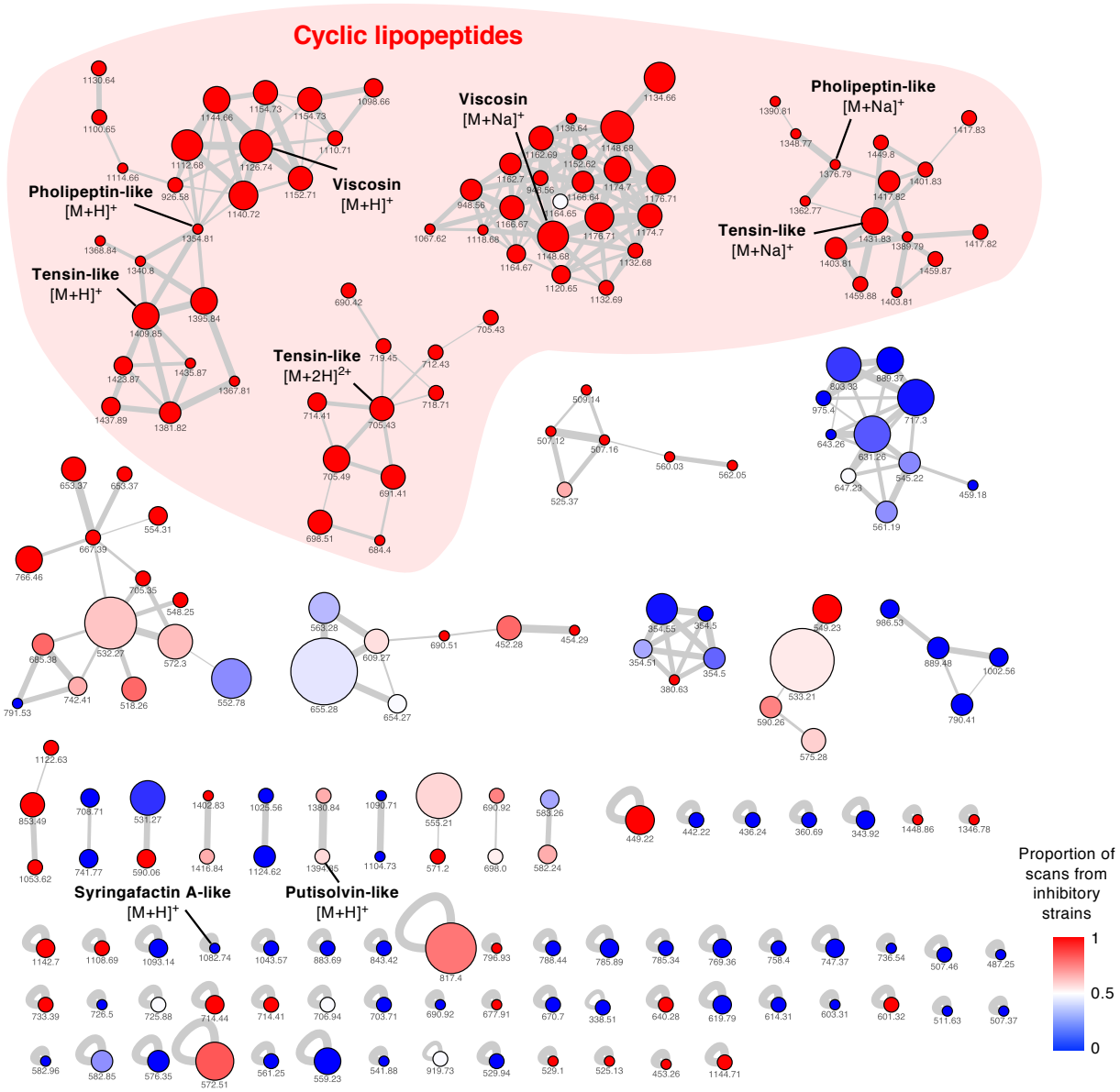

Figure 4 Mass spectral networking analysis of LC-MS^2 data from the *Pseudomonas* strains used in this study. Node area is proportional to the number of distinct strains where MS^2 data was acquired for a given metabolite. Node colour reflects the proportion of MS^2 scans for a given node that come from strains with a *S. scabies* inhibition score ≥1. Nodes are labelled with the corresponding parent masses and nodes that relate to lipopeptides are labelled (multiple networks arise from differential fragmentation of $[M+H]^+$, $[M+2H]^{2+}$ and $[M+Na]^+$ ions). Line thickness is proportional to the cosine similarity score calculated by GNPS (65).

To assess the potential role of CLPs in mediating the interaction between *P. fluorescens* and *S. scabies*, an NRPS gene predicted to be involved in the biosynthesis of a viscosin-like molecule in Ps682 was deleted by allelic replacement (Figure 5A). The resulting Ps682 Δ*visc* strain was unable to make the viscosin-like molecule (*m/z* 1126.69, Figure 5B), or to undergo swarming motility (Figure S17). This is in agreement with earlier work on the role of viscosin in the motility of *P. fluorescens* SBW25 (58) and the observation that possession of a CLP gene cluster was

309 the genotype that most strongly correlated with motility (ρ = 0.65, Figure S8). A cross-streak
310 assay with *S. scabies* (Figure 5C) revealed an active role for this CLP in on-plate *S. scabies*
311 inhibition (Figure 5C). Wild type (WT) Ps682 appeared to specifically colonise the *S. scabies*
312 streak, whereas Ps682 Δ*visc* was unable to restrict *S. scabies* growth. Alternatively, it was
313 possible that this instead could reflect diffusible inhibition of *Streptomyces* development by WT
314 Ps682, leading to a "bald" *S. scabies* phenotype (67). To distinguish between these possible
315 inhibition modes, a constitutively-expressed *lux* operon was integrated into the chromosomal
316 *att::*Tn*7* site (68) of Ps682 to visualise this interaction by bioluminescence. This clearly showed
317 viscosin-dependent *Pseudomonas* colonisation of the *Streptomyces* streaks (Figure 5C).
318

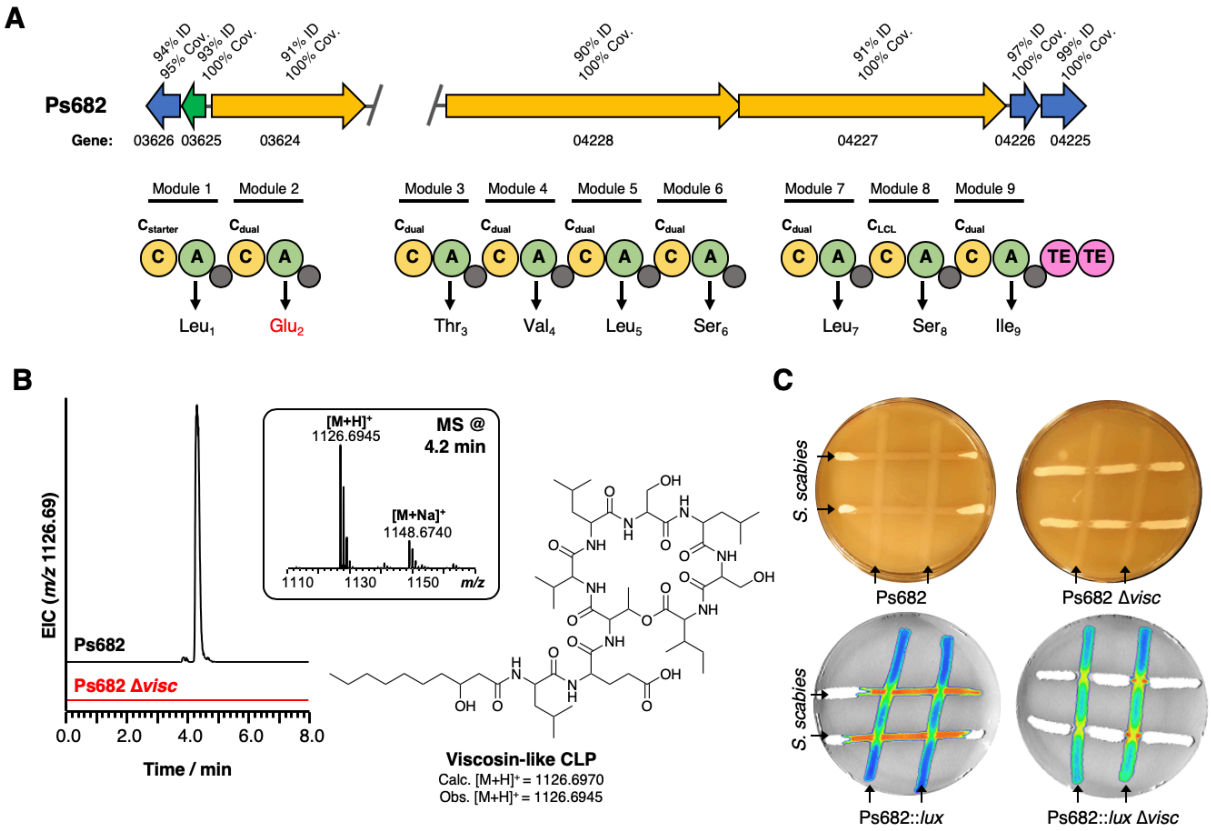

319

320 **Figure 5** The role of the Ps682 CLP gene cluster in *S. scabies* suppression. (A) BGC showing
321 homology to the *P. fluorescens* SBW25 viscosin BGC. Genes encoding regulatory proteins are green,
322 transporter genes are blue, and NRPS genes are yellow. The NRPS organization is shown, where C =
323 condensation domain, A = adenylation domain, TE = thioesterase, and small grey circles are peptidyl
324 carrier protein domains. Amino acids incorporated by each module are displayed (red indicates where
325 the antiSMASH prediction either does not correspond to the structure). (B) LC-MS analysis of CLP
326 production in the WT strain and a mutant (Ps682 Δ*visc*) with an in-frame deletion of NRPS gene 04228.
327 The predicted structure is based on MS^2 analysis and comparison to a viscosin standard produced by *P.*
328 *fluorescens* SBW25 (Figures S10 and S11). (C) On-plate *S. scabies* suppression activity of Ps682
329 alongside Ps682 Δ*visc* shown as cross-streaks using strains with and without the *lux* operon. Colour in
330 the lower plates indicates bioluminescence detected using a NightOWL camera (Berthold Technologies).

331

332 **Hydrogen cyanide and CLP production both contribute to *S. scabies* inhibition**

333 Pan-genome analysis showed that HCN production was predicted for a significant number of
334 suppressive strains (ρ = 0.47, Figure S8), where 17 of the 19 strains containing HCN gene
335 clusters were inhibitory towards *S. scabies* (Figure 2). The HCN pathway is encoded by the
336 *hcnABC* gene cluster (Figure S9) and has previously been associated with insect and fungal
337 pathogen inhibition in other *Pseudomonas* strains (19, 27, 69). HCN is toxic to a wide variety of
338 organisms, but not to *Pseudomonas* owing to their branched aerobic respiratory chain that has
339 at least five terminal oxidases, including a cyanide-insensitive oxidase (70, 71). We confirmed
340 that nearly every strain with the *hcnABC* gene cluster produced HCN (18 out of 19) using the
341 Feigl Anger colorimetric detection reagent (72) (Supporting Dataset 1) and used this assay to
342 identify HCN producers across the original collection of 240 *Pseudomonas* strains. This wider
343 analysis showed that HCN production strongly correlated with *S. scabies* inhibition (ρ = 0.52,
344 Figure S18), in accordance with our analysis of the sequenced strains.

345

346 To examine the role of HCN in *S. scabies* suppression and whether it exhibited a synergistic
347 effect with lipopeptide production, Ps619 was investigated as this strain produces both HCN
348 and a tensin-like compound (Figure 2 and Figure 6A). A tensin BGC has not previously been
349 reported, but the predicted amino acid specificity, mass (Figure 6A) and MS^2 fragmentation
350 (Figure S12) indicated that seven isolates produce tensin-like CLPs (Figure 3D). The *hcn* and
351 *ten* gene clusters were inactivated by in-frame deletions to generate single and double mutants
352 of Ps619, and the resulting Δ*hcn*, Δ*ten* and Δ*hcn*Δ*ten* mutants were subjected to cross-streak
353 assays (Figure 6B). A comparison of wild type, single and double mutants showed that HCN
354 inhibits *S. scabies* growth and development across the entire plate, while tensin is important for
355 *Pseudomonas* motility and helps the *Pseudomonas* to grow competitively at the cross-streak
356 interface. Furthermore, this suppressive effect is additive: the Ps619 Δ*hcn* and Δ*ten* single
357 mutants both retained some inhibitory activity towards *S. scabies*, whereas the Ps619 Δ*hcn*Δ*ten*
358 double mutant could not inhibit *S. scabies*.

359

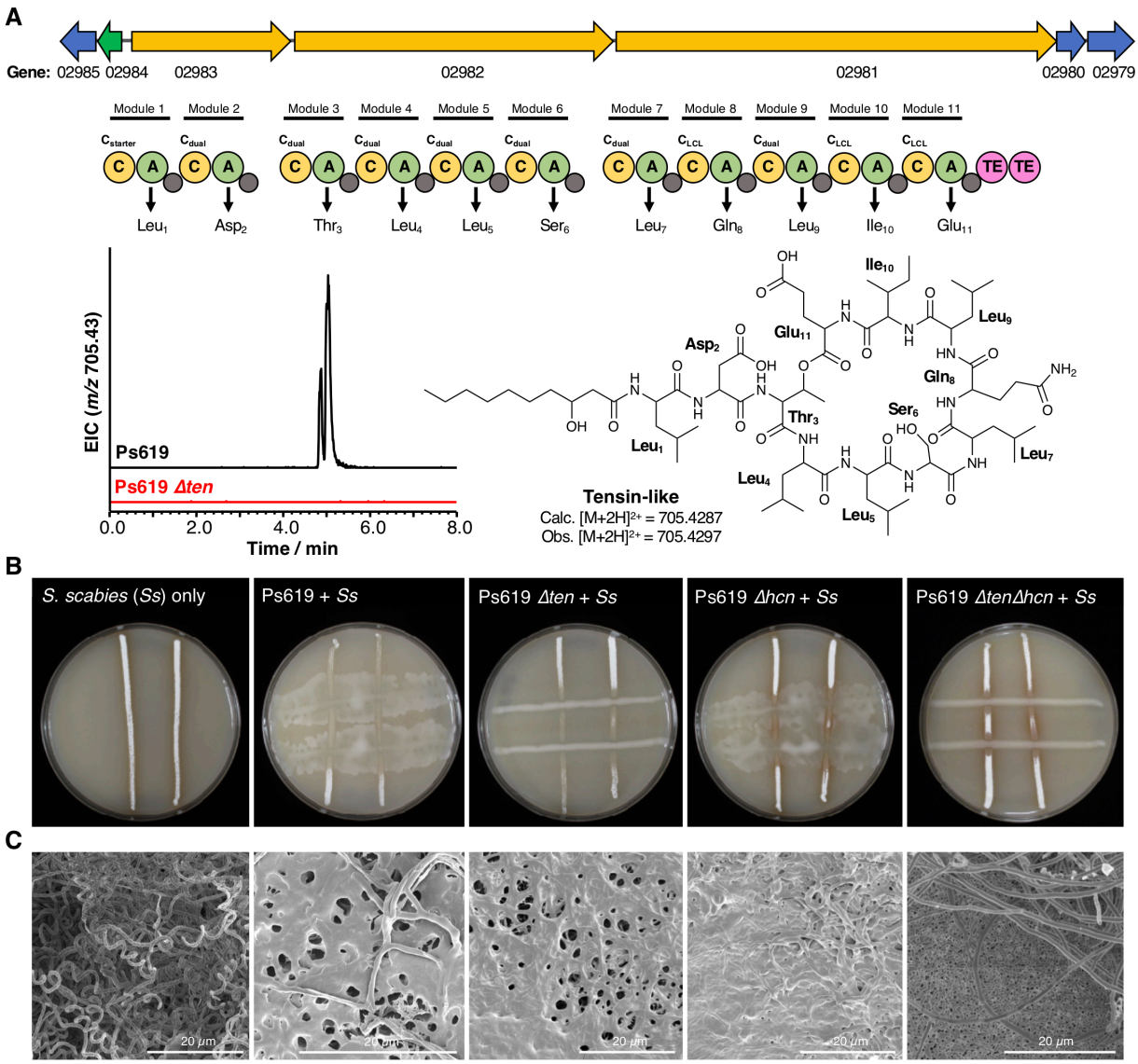

Figure 6 The role of the Ps619 CLP and HCN gene clusters in *S. scabies* suppression. (A) Organisation of the CLP NRPS from Ps619 alongside a predicted structure of the tensin-like molecule and LC-MS analysis of CLP production in WT Ps619 and a mutant (Ps619 Δ*ten*) with an in-frame deletion of NRPS gene 02981. (B) Cross streak assays of Ps619 and associated mutants with *S. scabies*. (C) CryoSEM images of the interfacial region between the Ps619 strains and *S. scabies*. The order of images is identical to the cross-streaks in panel B.

In drier growth conditions expected to favour streptomycete growth and limit motility, the role of tensin-mediated motility was abrogated, yet tensin and HCN still possessed an additive inhibitory effect at the microbial interface (Figure S19). Notably, Ps619 Δ*hcn* was able to induce a developmental defect in *S. scabies* at the microbial interface that was not present in Ps619 Δ*ten* or Ps619 Δ*hcn*Δ*ten*, showing that the tensin-like CLP induces a developmental defect in *S. scabies* that is independent of *Pseudomonas* motility. This analysis also clearly showed that at areas distant from the bacterial interaction, *S. scabies* grew more vigorously when cultured

375 with Δ*hcn* strains, consistent with the volatility of HCN enabling a long-range inhibitory effect. A
376 similar volatile effect was seen when Ps619 strains were separated from *S. scabies* by a barrier,
377 where only those strains producing HCN inhibited growth and development (Figure S19).
378
379 To further probe how tensin and HCN affected the interaction between Ps619 strains and *S.*
380 *scabies*, the interfacial regions of cross-streaks were imaged using Cryo-scanning electron
381 microscopy (CryoSEM). WT Ps619 was able to colonise the *S. scabies* streak meaning that the
382 interfacial region imaged was further from the cross-streak intersection than all other co-cultures
383 (Figure 6C). Here, Ps619 inhibited *S. scabies* development, which appears as a mixture of
384 deformed aerial hyphae and vegetative growth reminiscent of a "bald" phenotype (73, 74).
385 CryoSEM indicated that both the Ps619 Δ*hcn* and Δ*ten* mutants induced a similar partially bald
386 phenotype in *S. scabies*, but the Δ*hcn*Δ*ten* double mutant was unable to trigger the same
387 developmental defect, as *S. scabies* could develop aerial mycelia close to the microbial
388 interface (Figure 6C and Figure S20). This appears as a clear boundary between Ps619
389 Δ*hcn*Δ*ten* (single cells in background, bottom right panel of Fig 6C) and *S. scabies* (hyphae in
390 the foreground). The volatile HCN can inhibit growth and development at a distance, whereas
391 CLP inhibition of development only occurs close to the microbial interface. Both inhibitory
392 mechanisms enable Ps619 to obtain a competitive advantage at the microbe-microbe interface
393 (Figure 6C and Figure S20), while the CLP also functions as a surfactant enabling Ps619
394 motility, promoting *Pseudomonas* invasion of the *Streptomyces* cross-streak.
395
396 **A subset of *P. fluorescens* strains are generalist pathogen suppressors**
397 To determine whether the strains and metabolites we identified specifically suppress *S. scabies*
398 or have suppressive activity towards a range of plant pathogens, we investigated the ability of
399 the potato field strain collection to suppress the growth of the destructive plant pathogens
400 *Phytophthora infestans*, the oomycete that causes potato blight (75), and *Gaeumannomyces*
401 *graminis* var. *tritici*, the fungus that causes take-all disease of cereal crops (18). Notably, this
402 revealed strong positive correlations between suppressive phenotypes for each of the
403 pathogens tested (a correlation coefficient of 0.55 between *S. scabies* and *P. infestans*
404 inhibition, Figure S8). More generally, there was strong congruence between the genotypes that
405 correlated (positively and negatively) with suppression of each pathogen (Figure 7A).
406
407 HCN and CLPs have both previously been identified as inhibitors of oomycete and fungal
408 growth(19, 26). To assess whether these natural products are critical for inhibition of *P. infestans*
409 and *G. graminis* by Ps619 and Ps682, our HCN/CLP mutants were tested for inhibitory activity
410 (Figure 7). Surprisingly, neither HCN or tensin were required for Ps619 inhibition of either *G.*
411 *graminis* (Figure 7B) or *P. infestans* (Figure S21), indicating the production of at least one other

412 secreted inhibitory factor. In contrast, inactivation of the viscosin-like pathway in Ps682
413 abolished bioactivity towards both pathogens (Figure 7C). These data indicate that a subset of
414 pseudomonads can function as generalist pathogen suppressors, possessing multiple growth
415 inhibition mechanisms (e.g. Ps619) and/or by producing molecules with broad bioactivity (e.g.
416 Ps682).
417

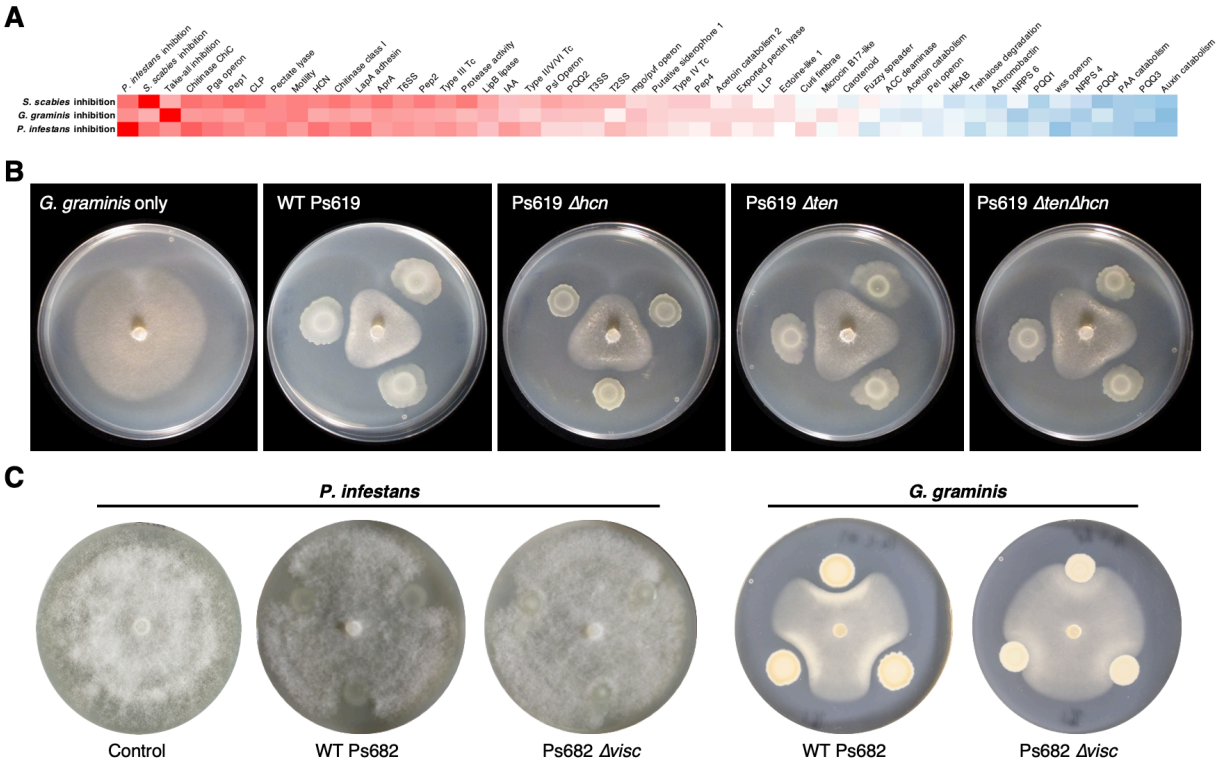

418

419 **Figure 7** *Pseudomonas* suppression of *P. infestans* and *G. graminis*. (A) Heatmap of Pearson
420 correlation coefficients of pathogen inhibition versus genotypes and phenotypes (see Figure S8 for full
421 correlations). The same colour scale as Figure 3A is used. (B) On-plate inhibition of *G. graminis* growth
422 by WT and mutant Ps619 strains. See Figure S21 for an analysis of *P. infestans* growth. (C) WT and
423 mutant Ps682 activity towards *P. infestans* and *G. graminis*.
424

425 Multiple accessory genome loci (Figure 7A) are strongly correlated with pathogen suppression
426 and these are often associated with the same subset of strains (Figure 3C). These loci include
427 chitinases (76), the extracellular alkaline metalloprotease AprA (77) and the *pga* operon, which
428 produces the biofilm structural polymer poly-β-1,6-N-acetyl-D-glucosamine (78).
429 Phenotypically, extracellular protease activity also positively correlates with suppression. The
430 gene cluster that correlated most strongly with *S. scabies* suppression was Pep1 ("Peptide 1"),
431 while the related Pep2 also correlated strongly (ρ = 0.57 and 0.50, respectively, Figure 3A).
432 These were identified by antiSMASH as putative "bacteriocin" BGCs, as they encode short
433 peptides (DUF2282 family) alongside DUF692 and DUF2063 proteins (Figure S9). Nothing is
434 known about DUF2282 peptides, whereas the DUF692 protein family includes MbnB, which

435 was recently characterised as a dioxygenase involved in methanobactin biosynthesis (79) and
436 PmaH, an iron-dependent dioxygenase involved in the biosynthesis of 3-thiaglutamate in
437 *Pseudomonas syringae* (80). Studies in other bacteria indicate that DUF692 and DUF2063 may
438 be involved in a heavy metal and/or oxidative stress responses (81-83). Further work is ongoing
439 to determine the significance of both the Pep gene clusters and the accessory genome loci for
440 pathogen inhibition.
441
442 **The effect of irrigation on the soil *Pseudomonas* population**
443 Irrigation is currently the only effective way to control potato scab, so we hypothesised that this
444 may lead to an increase in the number of inhibitory bacteria associated with the soil and/or
445 tuber, especially as the *Pseudomonadales* population moderately increased in irrigated soil
446 (Figure 1C). Interestingly however, a greater number of strongly suppressive strains (inhibition
447 score ≥ 2) were isolated from non-irrigated sites (7/60 strains) than from irrigated sites (1/60
448 strains). A similar pattern was observed for strongly motile (score ≥ 2) strains (6 non-irrigated
449 versus 2 irrigated). Analysis of the natural product gene clusters in our sequenced strains
450 revealed a similar result, where 5/18 unirrigated strains contained CLP BGCs versus 0/16
451 irrigated strains. This counter-intuitive observation led us to hypothesise that irrigation enables
452 non-motile, non-suppressive bacteria to survive and colonise plant roots, whereas highly motile
453 bacteria that produce multiple biological weapons can more effectively colonise plants in drier,
454 more 'hostile' conditions.
455
456 To test these hypotheses, we sampled irrigated and unirrigated sites in a neighbouring field two
457 years after the first sampling event. 48 strains were isolated from bulk soil and the rhizospheres
458 of tuber-forming potato plants, with and without irrigation, providing a total of 192 *P. fluorescens*
459 strains (Supporting Dataset 1). These strains were scored for motility, HCN production and *S.*
460 *scabies* suppression (Figure 8A). Our results were in strong agreement with the first sample
461 set, including strong positive correlations between *S. scabies* inhibition, motility and HCN
462 production (Figure 8B). Pseudomonads with these traits were more likely to be found in the
463 rhizosphere, and this was more pronounced in the unirrigated samples, where statistically
464 significant differences (p-values <0.001) between the root and soil populations were observed
465 for each trait (Figure 8A). In addition, analysis of the samples isolated from roots showed that
466 motility, HCN production and *S. scabies* suppression were all negatively correlated with
467 irrigation, but these correlations were not observed in the strains isolated from bulk soil (Figure
468 8B).

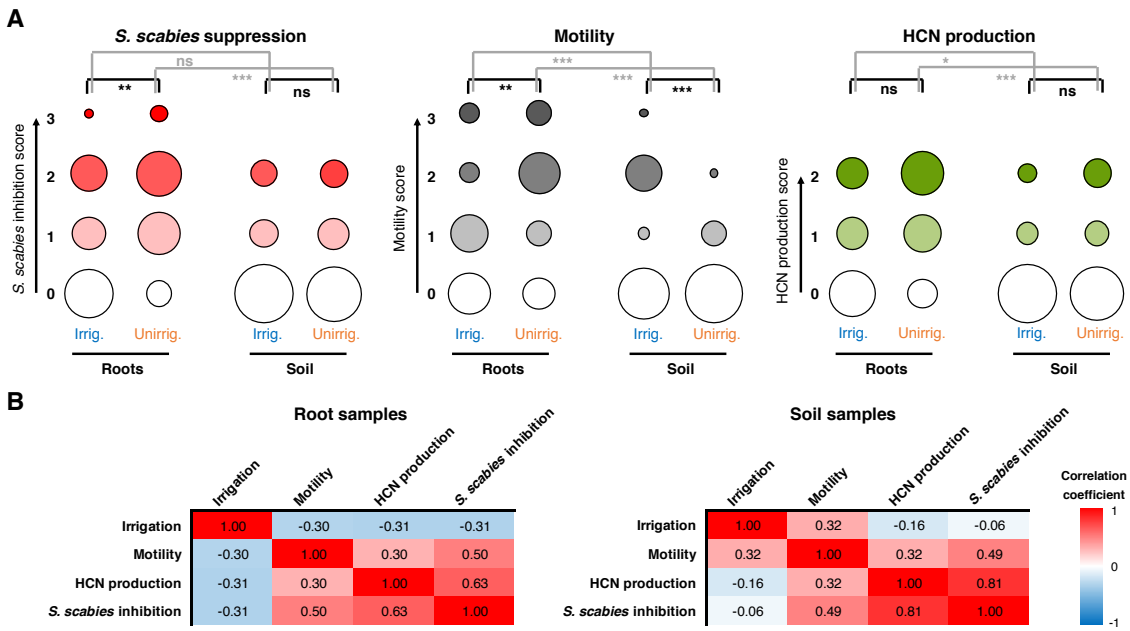

Figure 8 The effect of irrigation and environment (soil versus root) on the *P. fluorescens* population. (A) Plots showing the proportion of strains exhibiting a particular phenotype from each environment (n = 48 for each condition). HCN production was scored on a scale of 0-2 based on a qualitative assessment of the colour change in the Feigl Anger assay. The size of each circle is proportional to the number of strains with a given phenotypic score. Statistical comparisons were carried out using chi-squared tests where ns (not significant) = p≥0.05, * = p<0.05, ** = p<0.01, *** = p<0.001. (B) Pearson correlation scores for phenotypes from strains isolated from roots (n = 96) and soil (n = 96).

This analysis therefore supports the root colonisation hypothesis, where a lack of irrigation leads to a more specialised pseudomonad population colonising the root. Upon irrigation, the difference between the bulk soil and root pseudomonad populations is much less significant. The mechanism for this population change is not yet defined and these changes are counter-intuitive in relation to the suppression of potato scab upon irrigation, given there is a drop in suppressive strains colonising the potato root following irrigation. It is possible that a protective microbiome in irrigated conditions actually contains a mixture of *S. scabies*-suppressive "biocontrol" *Pseudomonas* strains alongside other non-motile pseudomonads that interact with the plant in important ways due to traits usually absent from the "biocontrol" strains, such as their ability to produce PQQ and catabolise auxins (54, 84).

Discussion

Prior studies on the suppression of potato scab have indicated a potential biocontrol role for *Pseudomonas* bacteria (20, 28, 29). Fluorescent pseudomonads form multiple beneficial relationships with plants, including growth promotion and biocontrol (9, 85). However, there is limited understanding of the genetic factors that are critical for such activity, and little is known about the diversity of the *P. fluorescens* species group within a given agricultural field or how

495 this population is shaped by environmental changes. In this study, we integrated genomics,
496 metabolomics, phenotypic analysis and molecular biology to identify the genetic determinants
497 of *Pseudomonas* antagonism towards *S. scabies*. This population level approach shows that
498 the *P. fluorescens* population in a single field is highly complex, heterogeneous and dynamic
499 (Figures 2, 3 and 8). The genetic and metabolic diversity of various genera or species groups
500 have previously been investigated in detail for several bacteria, including *Salinospora*(86),
501 *Rhodococcus* (87) and *Pseudoalteromonas* (88), *Burkholderia* (89) as well as prior studies on
502 *P. fluorescens* (7, 14, 15) and wider analyses of prokaryote secondary metabolism (41) and its
503 biogeographic distribution (90). However, these studies typically focus on the biosynthetic
504 capacity and associated phylogenetic relationships of globally distributed strains rather than
505 addressing the distribution and dynamics of natural product production for bacteria within a
506 defined geographic region.
507
508 Multiple biosynthetic gene clusters and accessory genome loci were identified that correlated
509 with on-plate inhibition of *S. scabies* growth and development (Figure 3), including BGCs for
510 cyclic lipopeptides and hydrogen cyanide. These loci also correlated with inhibition of *P.*
511 *infestans* and *G. graminis*, and their contribution to suppression was validated genetically. This
512 confirmed a role for both molecules in *S. scabies* inhibition (Figures 5 and 6), representing a
513 new function for these *Pseudomonas* specialized metabolites. Co-culture assays and CryoSEM
514 imaging (Figure 6C) showed that HCN and cyclic lipopeptides produced by Ps619 arrest the
515 formation of streptomycete aerial hyphae and subsequent sporulation, providing the
516 pseudomonad with a competitive advantage at the microbial interface. The roles of the CLPs
517 are reminiscent of the interaction between *B. subtilis* and *Streptomyces coelicolor*, where
518 surfactin functions as a surfactant required for the formation of aerial structures in *B. subtilis*
519 and arrests aerial development in *S. coelicolor* (59). Collectively, these results are surprising
520 given that streptomycetes themselves use surfactants to assist in the erection of aerial mycelia
521 (91, 92) and point to secondary antagonistic roles for these molecules beyond the reduction of
522 surface tension.
523
524 HCN and CLPs have also been associated with insect (27) and nematode (69) killing and the
525 suppression of other pathogenic fungi (26, 93). This indicates that a subset of pseudomonads
526 are generalist suppressors of pathogens (and presumably also non-pathogenic organisms) due
527 to the production of these broad range antimicrobials. Genetic analysis indicates that these
528 strains are more likely to encode the biosynthetic potential to make multiple suppressive
529 metabolites and proteins. Evidence for this is provided by the inhibition of both *P. infestans* and
530 *G. graminis* by Ps619 Δ*hcn*Δ*ten* (Figure 7B and Figure S21). A recent comprehensive study of
531 the inhibitory properties of bacteria associated with the *Arabidopsis* leaf microbiome showed

532 that a large proportion of the total inhibitory activity was due to *Pseudomonadales* bacteria and
533 that a subset of individual strains were active against a wide array of bacteria (94).
534
535 Unexpectedly, irrigation led to a decrease in the proportion of suppressive pseudomonads on
536 potato roots (Figure 8A) even though irrigation is one of the most effective ways to suppress
537 potato scab. There are multiple possible reasons for this discrepancy. Recruitment of non-
538 suppressive pseudomonads to the rhizosphere may benefit the plant in other ways, given that
539 they are more likely to modulate auxin biosynthesis (Figures 2 and 3A). For example, Cheng *et*
540 *al.* used transposon mutagenesis in the rhizobacterium *P. fluorescens* Pf.SS101 to show that
541 auxin biosynthesis was linked to plant growth promotion and induced systemic resistance, but
542 found no link with volatile or lipopeptide biosynthesis (6), while Mauchline *et al.* (18) also
543 observed a negative correlation between genes for viscosin production and plant hormone
544 manipulation pathways. It is also possible that irrigation enables *Pseudomonas* to out-compete
545 *S. scabies* in the rhizosphere due to relative fitness in wet conditions. While our study was
546 focused on fluorescent pseudomonads, interactions between these bacteria and the wider
547 microbiome (Figure 1) may also have a key role in potato scab suppression.
548
549 Moving forward, systematic analyses of individual organisms within microbiomes will continue
550 to help answer questions relating to microbial communities and host interactions that are difficult
551 to address using global 'omics approaches alone (32). For example, the role of many bacterial
552 specialized metabolites in nature is poorly understood, especially for prolific producers such as
553 the pseudomonads and the streptomycetes. Future studies could examine whether the host
554 selects for bacterial populations enriched in specific biosynthetic gene clusters and whether
555 environmental stimuli modulate the abundance of these gene clusters. Synthetic microbial
556 communities based on well-characterized natural communities could then be used to test
557 hypotheses on the role of specialized metabolites in shaping the community or modulating the
558 health of the host organism.
559

560 Materials and Methods

561

562 Strains and growth conditions

563 All strains used in this study are listed in Table S1. Unless otherwise stated, chemicals were
564 purchased from Sigma-Aldrich, enzymes from New England Biolabs, and molecular biology kits
565 from GE Healthcare and Promega. All *P. fluorescens* strains were grown at 28 °C in L medium
566 (Luria base broth, Formedium) and *Escherichia coli* at 37 °C in lysogeny broth (LB) (95). 1.3%
567 agar was added for solid media. Gentamicin was used at 25 µg/mL, carbenicillin at 100 µg/mL
568 and tetracycline (Tet) at 12.5 µg/mL.

569

570 **Soil sample collection**

571 Soil samples were collected from potato fields at RG Abrey Farms (East Wretham, Norfolk,
572 U.K., 52.4644° N, 0.8299° E). The first sampling was conducted in 2015 from two adjacent plots
573 in a single field. Soil samples were taken on 22nd January 2015, immediately prior to planting.
574 One plot was then covered loosely in polythene to protect it from irrigation. The same field sites
575 were sampled again in May at the point of maximum scab impact, once potato tubers had begun
576 to form. In this case soil samples were taken from the base of the plants, near the root system.
577 For each sampling event, a total of 12 samples were taken from three parallel potato beds at
578 regularly spaced intervals approximately one metre apart. For the second experiment, 12
579 irrigated and 12 non-irrigated potato plants were uprooted from field sites in June 2017 and
580 returned to the laboratory in large pots. Bulk soil samples were taken from these pots alongside
581 an equivalent number of rhizosphere-associated samples, which were defined as isolated root
582 systems gently shaken to remove bulk soil before processing as below. Samples were collected
583 in sterile 50 mL tubes and stored at 4 °C.

584

585 **Isolation of soil *Pseudomonas***

586 Sample processing was conducted at 4 °C throughout. 10 mL of sterile phosphate-buffered
587 saline (PBS, per litre: 8 g NaCl, 0.2 g KCl, 1.44 g Na_2HPO_4, 0.24 g KH_2PO_4, pH 7.4) were added
588 to 50 mL tubes containing 20 g of soil or root material, and vortexed vigorously for 10 minutes.
589 Samples were then filtered through a sterile muslin filter to remove larger debris. The resulting
590 suspension of soil and organic matter was centrifuged at 1000 rpm for 30 s to pellet remaining
591 soil particles, before serial dilution in PBS and plating on *Pseudomonas* selective agar. The
592 selection media comprised *Pseudomonas* agar base (Oxoid, UK) supplemented with CFC
593 (cetrimide/fucidin/cephalosporin) *Pseudomonas* selective supplement (Oxoid, UK). Plates were
594 incubated at 28 °C until colonies arose, then isolated single colonies were patched on fresh
595 CFC agar and incubated overnight at 28 °C before streaking to single colonies on King's B (KB)
596 agar plates (96). Six isolates were selected at random per soil sample and subjected to
597 phenotypic/genomic analysis.

598

599 **Amplicon sequencing**

600 Genomic DNA was isolated from 3 g of pooled soil samples using the FastDNA™ SPIN Kit for
601 soil (MP Biomedicals, UK) following the manufacturer's instructions. Genomic DNA
602 concentration and purity was determined by NanoDrop spectrophotometry as above. Microbial
603 16S rRNA genes were amplified from soil DNA samples with barcoded universal prokaryotic

604 primers (515F/R806) targeting the V4 region, and then subjected to Illumina® MiSeq
605 sequencing (600-cycle, 2x300 bp) at the DNA Sequencing Facility, Department of Biochemistry,
606 University of Cambridge (UK). The data was analysed using the MiSeq Reporter Metagenomics
607 Workflow (Illumina, UK) to acquire read counts for all taxonomic ranks from phylum to genus.
608 MiSeq data were visualized and analysed using Degust 3.1.0 (http://degust.erc.monash.edu/)
609 and Pheatmap (https://CRAN.R-project.org/package=pheatmap) in R 3.5.1.
610
611 **Phenotypic assays**
612 *Swarming motility:* 0.5% KB agar plates were poured and allowed to set and dry for 1 hour in a
613 sterile flow chamber. Plates were then inoculated with 2 µL spots of overnight cultures and
614 incubated overnight at room temperature. The motility of each isolate was tested in triplicate
615 and scored from 0 (no motility) to 3 (high motility).
616 *Secreted protease activity:* 5 µL of overnight cultures were spotted onto KB plates containing
617 1.0% skimmed milk powder. Plates were incubated at 28 °C and photographed after 24 hours,
618 with individual isolates scored as protease positive (score = 2) or negative (score = 0).
619 *Hydrogen cyanide (HCN) production:* An adaptation of the method described in Castric *et al.*
620 (97) was used. *Pseudomonas* isolates were inoculated into 150 µL of liquid KB medium in
621 individual wells of a flat bottomed 96-well plate. The plates were then overlaid with Feigl-Anger
622 reagent paper (72), prepared as follows. Whatman 3MM chromatography paper was soaked in
623 Feigl-Anger detection reagent (5 mg/mL copper(II) ethyl acetoacetate and 5 mg/mL 4,4'-
624 methylenebis(N,N-dimethylaniline) dissolved in chloroform). After complete solvent
625 evaporation, the paper was placed under the plate lid and strains were grown at 28 °C overnight
626 with gentle shaking. The intensity of blue staining on the paper was then scored from 0 (no
627 colour) to 3 (high blue intensity). The same method was applied to isolates growing on agar
628 medium.
629 *Streptomyces scabies inhibition:* Two parallel lines of *S. scabies* 87-22 spores were streaked
630 onto SFM plates (98) using a sterile toothpick. These lines were then cross streaked with
631 overnight cultures of *Pseudomonas* isolates. Plates were incubated at 30 °C and the relative
632 performance of each species was assessed daily for 5 days.
633 *Phytophthora infestans inhibition:* Assays were conducted with *P. infestans* #2006-3920A (6-
634 A1) (The Sainsbury Laboratory, UK). This was maintained on rye agar medium supplemented
635 with 2% sucrose (C-RSA) (99) at 21 °C. C-RSA was filtered through muslin fabric to enable
636 clearer observation of oomycete growth. Three 10 µL drops of overnight cultures per
637 *Pseudomonas* isolate strain were placed equidistantly 15 mm from the edge of C-RSA plates.

638 A 3 mm plug from the leading edge of a *P. infestans* culture was then placed in the centre of
639 each plate and incubated for a further 7 days at 21 °C before scoring and imaging.
640 *Take-all inhibition:* Assays were conducted with *Gaeumannomyces graminis var. tritici* strain
641 NZ.66.12 (18). Three 10 µL drops of overnight *Pseudomonas* cultures per strain were placed
642 equidistantly 15 mm from the edge of Potato Dextrose Agar (PDA) plates and incubated for 24
643 hours at 28 °C. NZ.66.12 was cultured on PDA agar for five days at room temperature A 3 mm
644 plug from the leading edge of the NZ.66.12 culture was then placed in the centre of each plate
645 and incubated for a further five days at 22 °C before the extent of *Ggt* inhibition was assessed.
646
647 **DNA extraction and Illumina® genome sequencing**
648 Single colonies of each isolate to be sequenced were picked from L agar plates and grown
649 overnight in L medium. DNA was then extracted from 2 mL of cell culture using a GenElute™
650 Bacterial Genomic DNA Kit (Sigma-Aldrich, USA). DNA samples were subjected to an initial
651 quality check using a Nanodrop spectrophotometer (Thermo Scientific, Wilmington, DE, USA)
652 before submission for Nextera library preparation and paired-end read sequencing on the
653 Illumina® MiSeq platform (600-cycle, 2x300 bp) at the DNA Sequencing Facility, Department
654 of Biochemistry, University of Cambridge (UK). Reads from 35 pseudomonads collected in
655 February 2015 were assembled into genomes using MaSuRCA v3.2.6 (100) with the following
656 settings: GRAPH_KMER_SIZE=auto; USE_LINKING_MATES=1;
657 LIMIT_JUMP_COVERAGE=60; CA_PARAMETERS = ovlMerSize=30 cgwErrorRate=0.25
658 ovlMemory=4GB; NUM_THREADS=16; JF_SIZE=100000000;
659 DO_HOMOPOLYMER_TRIM=0. Reads from 32 samples collected in May 2015 were
660 assembled into genomes using SPAdes v3.6.2 (101) with k-mer flag set to -k
661 21,33,55,77,99,127. All assembly tasks were conducted using 16 CPUs on a 256 GB compute
662 node within the Norwich Bioscience Institutes (NBI) High Performance Computing cluster. An
663 additional strain from May 2015 (Ps925) was sequenced and assembled by MicrobesNG
664 (http://www.microbesng.uk), which is supported by the BBSRC (grant number BB/L024209/1).
665 The 69 assembled genome sequences were annotated using Prokka (102), which implements
666 Prodigal (103) as an open reading frame calling tool. Genome assemblies are available at the
667 European Nucleotide Archive (http://www.ebi.ac.uk/ena/) with the project accession
668 PRJEB34261.
669
670 **Phylogenetic and bioinformatic analysis**
671 The *gyrB* housekeeping gene sequence was identified in each newly sequenced genome by
672 BLAST comparison with the sequence of *gyrB* from *P. fluorescens* SBW25 (104). The *gyrB*

673 sequences from these strains and several reference strains were aligned using MUSCLE 3.8.31
674 (105) with default settings, then a maximum likelihood tree was calculated using FastTree MP
675 (106) using default parameters on the CIPRES portal (107). Genomes were subjected to
676 bioinformatic analysis as described in the Supplementary Information. Phylogenetic trees and
677 presence/absence data for accessory genes were visualised using Interactive Tree of Life v3
678 (108), with *Pseudomonas aeruginosa* PAO1 *gyrB* as the outgroup.
679
680 **Molecular biology procedures**
681 Cloning was carried out in accordance with standard molecular biology techniques. *P.*
682 *fluorescens* deletion mutants were constructed by allelic exchange as described previously
683 (109). Up- and downstream flanking regions (approx. 500 bp) to the target genes were amplified
684 using primers listed in Table S2. PCR products in each case were ligated into pTS1 (110)
685 between XhoI and BamHI. The resulting deletion vectors were transformed into the target
686 strains by electroporation, and single crossovers selected on L + Tet and re-streaked to isolate
687 single colonies. 100 mL cultures in L medium from single crossovers were grown overnight at
688 28 °C, then plated onto L + 10% sucrose plates to counter-select for double crossovers.
689 Individual colonies from these plates were then patched onto L plates ± Tet, with Tet-sensitive
690 colonies tested for gene deletion by colony PCR using primers external to the deleted gene in
691 each case (Table S2).
692
693 Luminescent-tagged strains were produced by introduction of the *Aliivibrio fischeri luxCDABE*
694 cassette into the neutral *att::Tn7* site in *Pseudomonas* chromosomes using the Tn7-based
695 expression system described in Choi *et al.* (68). Strains were electroporated with plasmids
696 pUC18-mini*Tn7*T-Gm-*lux* and the helper pTNS2, and transformant colonies were grown on solid
697 L medium + gentamicin for 2-3 days at 28 °C. Integration of the *lux* cassette into *Pseudomonas*
698 genomes was confirmed by PCR and with a luminometer. Luminescent cells were then tracked
699 using the NightOWL visualisation system (Berthold Technologies, Germany). All plasmids used
700 in this study are reported in Table S3.
701
702 **Liquid chromatography - mass spectrometry detection of lipopeptides**
703 *Pseudomonas* isolates were grown overnight in L medium (10 mL) for 16 hours at 28 °C. 100
704 µL of each culture was used to inoculate 40 mm diameter KB agar plates. Plates were incubated
705 for 24 hours at 28 °C, before the agar from each plate was decanted into a sterile 50 mL tube
706 and extracted with 10 mL 50% EtOH with occasional vortexing for 3 hours. 2 mL was taken from
707 each sample and centrifuged in 2 mL tubes for 5 min at 16,000 g. The supernatant was collected

708 and stored at -80 °C. Samples were diluted with an equal volume of water, then subjected to
709 LC-MS analysis using a Shimadzu Nexera X2 UHPLC coupled to a Shimadzu ion-trap time-of-
710 flight (IT-TOF) mass spectrometer. Samples (5 µL) were injected onto a Phenomenex Kinetex
711 2.6 µm XB-C18 column (50 x 2.1mm, 100Å), eluting with a linear gradient of 5 to 95%
712 acetonitrile in water + 0.1% formic acid over 6 minutes with a flow-rate of 0.6 mL/min at 40 °C.
713 Positive mode mass spectrometry data was collected between *m/z* 300 and 2000 with an ion
714 accumulation time of 10 ms featuring an automatic sensitivity control of 70% of the base peak.
715 The curved desolvation line temperature was 300 °C and the heat block temperature was 250
716 °C. MS/MS data was collected in a data-dependent manner using collision-induced dissociation
717 energy of 50% and a precursor ion width of 3 Da. The instrument was calibrated using sodium
718 trifluoroacetate cluster ions prior to every run.
719
720 A molecular network was created using the online workflow at the Global Natural Product Social
721 Molecular Networking (GNPS) site (https://gnps.ucsd.edu/) (65). The data was filtered by
722 removing all MS/MS peaks within +/- 17 Da of the precursor *m/z*. The data was then clustered
723 with MS-Cluster with a parent mass tolerance of 1 Da and a MS/MS fragment ion tolerance of
724 0.5 Da to create consensus spectra. Consensus spectra that contained less than 2 spectra were
725 discarded. A network was then created where edges were filtered to have a cosine score above
726 0.6 and more than 4 matched peaks. Further edges between two nodes were kept in the network
727 if each of the nodes appeared in each other's respective top 10 most similar nodes. The spectra
728 in the network were then searched against GNPS spectral libraries. The library spectra were
729 filtered in the same manner as the input data. All matches kept between network spectra and
730 library spectra were required to have a score above 0.7 and at least 4 matched peaks. Networks
731 were visualised using Cytoscape v2.8.3 and the data was manually filtered to remove duplicate
732 nodes (same *m/z* and retention time). The data is available as a MassIVE dataset at
733 ftp://massive.ucsd.edu/MSV000084283/ and the GNPS analysis is available here:
734 https://gnps.ucsd.edu/ProteoSAFe/status.jsp?task=51ac5fe596424cf88cfc17898985cac2
735
736 **Scanning electron microscopy**
737 Small pieces of the *Pseudomonas-Streptomyces* co-culture samples were excised from the
738 surface of agar plates and mounted on an aluminium stub using Tissue Tek^{R} (BDH Laboratory
739 Supplies, Poole, England). The stub was then immediately plunged into liquid nitrogen slush at
740 approximately -210 °C to cryo-preserve the material. The sample was transferred onto the
741 cryostage of an ALTO 2500 cryo-transfer system (Gatan, Oxford, England) attached to an FEI
742 Nova NanoSEM 450 (FEI, Eindhoven, The Netherlands). Sublimation of surface frost was

743 performed at -95 °C for three minutes before sputter coating the sample with platinum for 3 min
744 at 10 mA, at colder than -110 °C. After sputter-coating, the sample was moved onto the cryo-
745 stage in the main chamber of the microscope, held at -125 °C. The sample was imaged at 3 kV
746 and digital TIFF files were stored.
747
748

749 ## Acknowledgements

750 Financial support was provided by a Royal Society University Research Fellowship to AWT,
751 Biotechnology and Biological Sciences Research Council (BBSRC) BIO, MET, PH and MfN
752 Institute Strategic Programme grants (BB/J004553/1, BB/J004596/1, BBS/E/J/000PR9797 and
753 BBS/E/J/000PR9790, respectively) to the John Innes Centre (JIC), a JIC Institute Development
754 Grant and NPRONET Proof of Concept grant POC021. We thank Prof. Jonathan Jones (The
755 Sainsbury Laboratory) for providing *P. infestans* isolates and Dr Tim Mauchline (Rothamsted
756 Research) for providing *Ggt* NZ.66.12. We thank the JIC Bioimaging facility for their contribution
757 to this publication.
758

759 ## Conflict of Interest

760 The authors declare no conflict of interest.
761

762 ## References

763 1. Larkin RP, et al. (2011) Effects of different potato cropping system approaches and
764 water management on soilborne diseases and soil microbial communities.
765 *Phytopathology* 101:58–67.
766 2. Lerat S, Simao-Beaunoir A-M, Beaulieu C (2009) Genetic and physiological
767 determinants of *Streptomyces scabies* pathogenicity. *Mol Plant Pathol* 10:579–585.
768 3. Wanner LA (2006) A survey of genetic variation in *Streptomyces* isolates causing
769 potato common scab in the United States. *Phytopathology* 96:1363–1371.
770 4. Mendes R, et al. (2011) Deciphering the rhizosphere microbiome for disease-
771 suppressive bacteria. *Science* 332:1097–1100.
772 5. Berg G, Krause R, Mendes R (2015) Cross-Kingdom Similarities in Microbiome
773 Ecology and Biocontrol of Pathogens. *Front Microbiol* 6:1311.
774 6. Cheng X, et al. (2017) Genome-wide analysis of bacterial determinants of plant
775 growth promotion and induced systemic resistance by *Pseudomonas fluorescens*.
776 *Environ Microbiol* 19:4638–4656.

777 7. Loper JE, et al. (2012) Comparative Genomics of Plant-Associated *Pseudomonas*
778 spp.: Insights into Diversity and Inheritance of Traits Involved in Multitrophic
779 Interactions. *PLOS Genet* 8:e1002784.
780 8. Zamioudis C, Mastranesti P, Dhonukshe P, Blilou I, Pieterse CMJ (2013) Unraveling
781 Root Developmental Programs Initiated by Beneficial *Pseudomonas* spp. Bacteria.
782 *Plant Physiol* 162:304–318.
783 9. Haas D, Défago G (2005) Biological control of soil-borne pathogens by fluorescent
784 pseudomonads. *Nat Rev Micro* 3:307–319.
785 10. Weller DM (2007) *Pseudomonas* biocontrol agents of soilborne pathogens: looking
786 back over 30 years. *Phytopathology* 97:250–256.
787 11. Bakker PAHM, Pieterse CMJ, van Loon LC (2007) Induced Systemic Resistance by
788 Fluorescent *Pseudomonas* spp. *Phytopathology* 97:239–243.
789 12. Kwak Y-S, Weller DM (2013) Take-all of Wheat and Natural Disease Suppression: A
790 Review. *Plant Pathol J* 29:125–135.
791 13. Gross H, Loper JE (2009) Genomics of secondary metabolite production by
792 Pseudomonas spp. *Nat Prod Rep* 26:1408–1446.
793 14. Nguyen DD, et al. (2016) Indexing the *Pseudomonas* specialized metabolome
794 enabled the discovery of poaeamide B and the bananamides. *Nat Microbiol* 2:1–9.
795 15. Stringlis IA, Zhang H, Pieterse CMJ, Bolton MD, de Jonge R (2018) Microbial small
796 molecules - weapons of plant subversion. *Nat Prod Rep* 35:410–433.
797 16. Ghequire MGK, De Mot R (2014) Ribosomally encoded antibacterial proteins and
798 peptides from *Pseudomonas*. *FEMS Microbiol Rev* 38:523–568.
799 17. Rangel LI, et al. (2016) Characterization of Toxin Complex Gene Clusters and Insect
800 Toxicity of Bacteria Representing Four Subgroups of *Pseudomonas fluorescens*.
801 *PLOS One* 11:e0161120.
802 18. Mauchline TH, et al. (2015) An analysis of *Pseudomonas* genomic diversity in take-all
803 infected wheat fields reveals the lasting impact of wheat cultivars on the soil
804 microbiota. *Environ Microbiol* 17:4764–4778.
805 19. Hunziker L, et al. (2015) *Pseudomonas* strains naturally associated with potato plants
806 produce volatiles with high potential for inhibition of *Phytophthora infestans*. *Appl*
807 *Environ Microbiol* 81:821–830.
808 20. Arseneault T, Goyer C, Filion M (2013) Phenazine Production by *Pseudomonas* sp.
809 LBUM223 Contributes to the Biological Control of Potato Common Scab.
810 *Phytopathology* 103:995–1000.
811 21. Silby MW, et al. (2009) Genomic and genetic analyses of diversity and plant
812 interactions of *Pseudomonas fluorescens*. *Genome Biol* 10:R51.

22. Gomila M, Peña A, Mulet M, Lalucat J, García-Valdés E (2015) Phylogenomics and systematics in *Pseudomonas*. *Front Microbiol* 6:214.
23. Melnyk RA, Hossain SS, Haney CH (2019) Convergent gain and loss of genomic islands drive lifestyle changes in plant-associated *Pseudomonas*. *ISME J* 13:1575–1588.
24. Garrido-Sanz D, et al. (2016) Genomic and Genetic Diversity within the *Pseudomonas fluorescens* Complex. *PLOS One* 11:e0150183.
25. Turnbull GA, Morgan JAW, Whipps JM, Saunders JR (2001) The role of bacterial motility in the survival and spread of *Pseudomonas fluorescens* in soil and in the attachment and colonisation of wheat roots. *FEMS Microbiol Ecol* 36:21–31.
26. Michelsen CF, et al. (2015) Nonribosomal peptides, key biocontrol components for *Pseudomonas fluorescens* In5, isolated from a Greenlandic suppressive soil. *mBio* 6:e00079.
27. Flury P, et al. (2017) Antimicrobial and Insecticidal: Cyclic Lipopeptides and Hydrogen Cyanide Produced by Plant-Beneficial *Pseudomonas* Strains CHA0, CMR12a, and PCL1391 Contribute to Insect Killing. *Front Microbiol* 8:100.
28. Elphinstone JG, Thwaites R, Stalham M, Wale S (2009) Integration of precision irrigation and non-water based measures to suppress common scab of potato. Potato Council R272 Final Report.
29. Rosenzweig N, Tiedje JM, Quensen JF III, Meng Q, Hao JJ (2012) Microbial communities associated with potato common scab-suppressive soil determined by pyrosequencing analyses. *Plant Dis* 96:718–725.
30. Meng Q, Yin J, Rosenzweig N, Douches D, Hao JJ (2012) Culture-based assessment of microbial communities in soil suppressive to potato common scab. *Plant Dis* 96:712–717.
31. Hartmann M, et al. (2017) A decade of irrigation transforms the soil microbiome of a semi-arid pine forest. *Mol Ecol* 26:1190–1206.
32. Mauchline TH, Malone JG (2017) Life in earth - the root microbiome to the rescue? *Curr Opin Microbiol* 37:23–28.
33. Law CW, Chen Y, Shi W, Smyth GK (2014) voom: Precision weights unlock linear model analysis tools for RNA-seq read counts. *Genome Biol* 15:R29.
34. Weinert N, et al. (2011) PhyloChip hybridization uncovered an enormous bacterial diversity in the rhizosphere of different potato cultivars: many common and few cultivar-dependent taxa. *FEMS Microbiol Ecol* 75:497–506.
35. Pfeiffer S, et al. (2017) Rhizosphere microbiomes of potato cultivated in the High Andes show stable and dynamic core microbiomes with different responses to plant development. *FEMS Microbiol Ecol* 93:fiw242.

850 36. Blin K, et al. (2017) antiSMASH 4.0-improvements in chemistry prediction and gene
851 cluster boundary identification. *Nucleic Acids Res* 45:W36–W41.
852 37. Pessi G, Haas D (2000) Transcriptional control of the hydrogen cyanide biosynthetic
853 genes hcnABC by the anaerobic regulator ANR and the quorum-sensing regulators
854 LasR and RhlR in *Pseudomonas aeruginosa*. *J Bacteriol* 182:6940–6949.
855 38. Metelev M, Serebryakova M, Ghilarov D, Zhao Y, Severinov K (2013) Structure of
856 microcin B-like compounds produced by *Pseudomonas syringae* and species
857 specificity of their antibacterial action. *J Bacteriol* 195:4129–4137.
858 39. Medema MH, Takano E, Breitling R (2013) Detecting sequence homology at the gene
859 cluster level with MultiGeneBlast. *Mol Biol Evol* 30:1218–1223.
860 40. Raaijmakers JM, de Bruijn I, Nybroe O, Ongena M (2010) Natural functions of
861 lipopeptides from *Bacillus* and *Pseudomonas*: more than surfactants and antibiotics.
862 *FEMS Microbiol Rev* 34:1037–1062.
863 41. Cimermancic P, et al. (2014) Insights into secondary metabolism from a global
864 analysis of prokaryotic biosynthetic gene clusters. *Cell* 158:412–421.
865 42. Berti AD, Greve NJ, Christensen QH, Thomas MG (2007) Identification of a
866 biosynthetic gene cluster and the six associated lipopeptides involved in swarming
867 motility of *Pseudomonas syringae* pv. tomato DC3000. *J Bacteriol* 189:6312–6323.
868 43. Berti AD, Thomas MG (2009) Analysis of achromobactin biosynthesis by
869 *Pseudomonas syringae* pv. syringae B728a. *J Bacteriol* 191:4594–4604.
870 44. Matthijs S, Budzikiewicz H, Schäfer M, Wathelet B, Cornelis P (2008) Ornicorrugatin,
871 a new siderophore from *Pseudomonas fluorescens* AF76. *Z Naturforsch C* 63:8–12.
872 45. Mercado-Blanco J, et al. (2001) Analysis of the pmsCEAB gene cluster involved in
873 biosynthesis of salicylic acid and the siderophore pseudomonine in the biocontrol
874 strain *Pseudomonas fluorescens* WCS374. *J Bacteriol* 183:1909–1920.
875 46. Patel HM, Walsh CT (2001) In Vitro Reconstitution of the *Pseudomonas aeruginosa*
876 Nonribosomal Peptide Synthesis of Pyochelin: Characterization of Backbone
877 Tailoring Thiazoline Reductase and N-Methyltransferase Activities. *Biochemistry*
878 40:9023–9031.
879 47. Milne JC, et al. (1999) Cofactor Requirements and Reconstitution Of Microcin B17
880 Synthetase: A Multienzyme Complex that Catalyzes the Formation of Oxazoles and
881 Thiazoles in the Antibiotic Microcin B17. *Biochemistry* 38:4768–4781.
882 48. Kim SY, et al. (2012) Different biosynthetic pathways to fosfomycin in *Pseudomonas*
883 *syringae* and *Streptomyces* species. *Antimicrob Agents Chemother* 56:4175–4183.
884 49. Dischinger J, Basi Chipalu S, Bierbaum G (2014) Lantibiotics: promising candidates
885 for future applications in health care. *Int J Med Microbiol* 304:51–62.

886 50. Coulthurst SJ, Barnard AML, Salmond GPC (2005) Regulation and biosynthesis of
887 carbapenem antibiotics in bacteria. *Nat Rev Micro* 3:295–306.
888 51. Kudo F, Eguchi T (2009) Biosynthetic genes for aminoglycoside antibiotics. *J Antibiot*
889 62:471–481.
890 52. Rangaswamy V, Jiralerspong S, Parry R, Bender CL (1998) Biosynthesis of the
891 Pseudomonas polyketide coronafacic acid requires monofunctional and
892 multifunctional polyketide synthase proteins. *Proc Natl Acad Sci USA* 95:15469–
893 15474.
894 53. Puehringer S, Metlitzky M, Schwarzenbacher R (2008) The pyrroloquinoline quinone
895 biosynthesis pathway revisited: a structural approach. *BMC Biochem* 9:8.
896 54. Choi O, et al. (2008) Pyrroloquinoline quinone is a plant growth promotion factor
897 produced by *Pseudomonas fluorescens* B16. *Plant Physiol* 146:657–668.
898 55. Zachow C, et al. (2015) The Novel Lipopeptide Poaeamide of the Endophyte
899 *Pseudomonas poae* RE*1-1-14 Is Involved in Pathogen Suppression and Root
900 Colonization. *Mol Plant Microbe Interact* 28:800–810.
901 56. Hultberg M, Bengtsson T, Liljeroth E (2010) Late blight on potato is suppressed by the
902 biosurfactant-producing strain *Pseudomonas koreensis* 2.74 and its biosurfactant.
903 *BioControl* 55:543–550.
904 57. Jang JY, et al. (2013) Identification of orfamide A as an insecticidal metabolite
905 produced by *Pseudomonas protegens* F6. *J Agric Food Chem* 61:6786–6791.
906 58. Alsohim AS, et al. (2014) The biosurfactant viscosin produced by *Pseudomonas*
907 *fluorescens* SBW25 aids spreading motility and plant growth promotion. *Environ*
908 *Microbiol* 16:2267–2281.
909 59. Straight PD, Willey JM, Kolter R (2006) Interactions between *Streptomyces coelicolor*
910 and *Bacillus subtilis*: Role of surfactants in raising aerial structures. *J Bacteriol*
911 188:4918–4925.
912 60. Han JS, et al. (2005) Biological control agent of common scab disease by antagonistic
913 strain *Bacillus* sp. sunhua. *J Appl Microbiol* 99:213–221.
914 61. Nielsen TH, Thrane C, Christophersen C, Anthoni U, Sørensen J (2000) Structure,
915 production characteristics and fungal antagonism of tensin - a new antifungal cyclic
916 lipopeptide from *Pseudomonas fluorescens* strain 96.578. *J Appl Microbiol* 89:992–
917 1001.
918 62. Götze S, et al. (2017) Structure, Biosynthesis, and Biological Activity of the Cyclic
919 Lipopeptide Anikasin. *ACS Chem Biol* 12:2498–2502.
920 63. Kuiper I, et al. (2004) Characterization of two *Pseudomonas putida* lipopeptide
921 biosurfactants, putisolvin I and II, which inhibit biofilm formation and break down
922 existing biofilms. *Mol Microbiol* 51:97–113.

923 64. Pauwelyn E, et al. (2013) New linear lipopeptides produced by *Pseudomonas cichorii*
924 SF1-54 are involved in virulence, swarming motility, and biofilm formation. *Mol Plant*
925 *Microbe Interact* 26:585–598.
926 65. Wang M, et al. (2016) Sharing and community curation of mass spectrometry data
927 with Global Natural Products Social Molecular Networking. *Nat Biotechnol* 34:828–
928 837.
929 66. Nguyen DD, et al. (2013) MS/MS networking guided analysis of molecule and gene
930 cluster families. *Proc Natl Acad Sci USA* 110:E2611–E2620.
931 67. Flardh K, Buttner MJ (2009) *Streptomyces* morphogenetics: dissecting differentiation
932 in a filamentous bacterium. *Nat Rev Micro* 7:36–49.
933 68. Choi K-H, et al. (2005) A Tn7-based broad-range bacterial cloning and expression
934 system. *Nat Meth* 2:443–448.
935 69. Siddiqui IA, Shaukat SS, Sheikh IH, Khan A (2006) Role of cyanide production by
936 *Pseudomonas fluorescens* CHA0 in the suppression of root-knot nematode,
937 *Meloidogyne javanica* in tomato. *World J Microbiol Biotechnol* 22:641–650.
938 70. Ugidos A, Morales G, Rial E, Williams HD, Rojo F (2008) The coordinate regulation of
939 multiple terminal oxidases by the *Pseudomonas putida* ANR global regulator. *Environ*
940 *Microbiol* 10:1690–1702.
941 71. Comolli JC, Donohue TJ (2002) *Pseudomonas aeruginosa* RoxR, a response
942 regulator related to *Rhodobacter sphaeroides* PrrA, activates expression of the
943 cyanide-insensitive terminal oxidase. *Mol Microbiol* 45:755–768.
944 72. Feigl F, Anger V (1966) Replacement of benzidine by copper ethylacetoacetate and
945 tetra base as spot-test reagent for hydrogen cyanide and cyanogen. *Analyst* 91:282–
946 284.
947 73. Tschowri N, et al. (2014) Tetrameric c-di-GMP mediates effective transcription factor
948 dimerization to control *Streptomyces* development. *Cell* 158:1136–1147.
949 74. Tschowri N (2016) Cyclic Dinucleotide-Controlled Regulatory Pathways in
950 *Streptomyces* Species. *J Bacteriol* 198:47–54.
951 75. Nowicki M, Foolad MR, Nowakowska M, Kozik EU (2011) Potato and Tomato Late
952 Blight Caused by *Phytophthora infestans*: An Overview of Pathology and Resistance
953 Breeding. *Plant Dis* 96:4–17.
954 76. Folders J, et al. (2001) Characterization of *Pseudomonas aeruginosa* chitinase, a
955 gradually secreted protein. *J Bacteriol* 183:7044–7052.
956 77. Laarman AJ, et al. (2012) *Pseudomonas aeruginosa* alkaline protease blocks
957 complement activation via the classical and lectin pathways. *J Immunol* 188:386–393.

958 78. Itoh Y, et al. (2008) Roles of pgaABCD genes in synthesis, modification, and export of
959 the *Escherichia coli* biofilm adhesin poly-beta-1,6-N-acetyl-D-glucosamine. *J Bacteriol*
960 190:3670–3680.
961 79. Kenney GE, et al. (2018) The biosynthesis of methanobactin. *Science* 359:1411–
962 1416.
963 80. Ting CP, et al. (2019) Use of a scaffold peptide in the biosynthesis of amino acid-
964 derived natural products. *Science* 365:280–284.
965 81. Clark IC, Melnyk RA, Iavarone AT, Novichkov PS, Coates JD (2014) Chlorate
966 reduction in *Shewanella algae* ACDC is a recently acquired metabolism characterized
967 by gene loss, suboptimal regulation and oxidative stress. *Mol Microbiol* 94:107–125.
968 82. Sarkisova SA, et al. (2014) A *Pseudomonas aeruginosa* EF-hand protein, EfhP
969 (PA4107), modulates stress responses and virulence at high calcium concentration.
970 *PLOS One* 9:e98985.
971 83. Price MN, et al. (2018) Mutant phenotypes for thousands of bacterial genes of
972 unknown function. *Nature* 557:503–509.
973 84. Spaepen S, Vanderleyden J (2011) Auxin and plant-microbe interactions. *Cold Spring*
974 *Harb Perspect Biol* 3:a001438.
975 85. Paterson J, et al. (2017) The contribution of genome mining strategies to the
976 understanding of active principles of PGPR strains. *FEMS Microbiol Ecol* 93:fiw249.
977 86. Ziemert N, et al. (2014) Diversity and evolution of secondary metabolism in the marine
978 actinomycete genus *Salinispora*. *Proc Natl Acad Sci USA* 111:E1130–E1139.
979 87. Ceniceros A, Dijkhuizen L, Petrusma M, Medema MH (2017) Genome-based
980 exploration of the specialized metabolic capacities of the genus *Rhodococcus*. *BMC*
981 *Genomics* 18:593.
982 88. Maansson M, et al. (2016) An Integrated Metabolomic and Genomic Mining Workflow
983 To Uncover the Biosynthetic Potential of Bacteria. *mSystems* 1:e00028–15.
984 89. Mullins AJ, et al. (2019) Genome mining identifies cepacin as a plant-protective
985 metabolite of the biopesticidal bacterium *Burkholderia ambifaria*. *Nat Microbiol* 4:996–
986 1005.
987 90. Charlop-Powers Z, et al. (2015) Global biogeographic sampling of bacterial secondary
988 metabolism. *eLife* 4:e05048.
989 91. Kodani S, et al. (2004) The SapB morphogen is a lantibiotic-like peptide derived from
990 the product of the developmental gene *ramS* in *Streptomyces coelicolor*. *Proc Natl*
991 *Acad Sci USA* 101:11448–11453.
992 92. Willey JM, Willems A, Kodani S, Nodwell JR (2006) Morphogenetic surfactants and
993 their role in the formation of aerial hyphae in *Streptomyces coelicolor*. *Mol Microbiol*
994 59:731–742.

995 93. Berry C, Fernando WGD, Loewen PC, de Kievit TR (2010) Lipopeptides are essential
996 for *Pseudomonas* sp. DF41 biocontrol of Sclerotinia sclerotiorum. *Biol Control*
997 55:211–218.
998 94. Helfrich EJN, et al. (2018) Bipartite interactions, antibiotic production and biosynthetic
999 potential of the *Arabidopsis* leaf microbiome. *Nat Microbiol* 3:909–919.
1000 95. Miller JH (1972) *Experiments in Molecular Genetics* (Cold Spring Harbor Laboratory,
1001 New York).
1002 96. King EO, Ward MK, Raney DE (1954) Two simple media for the demonstration of
1003 pyocyanin and fluorescin. *J Lab Clin Med* 44:301–307.
1004 97. Castric KF, Castric PA (1983) Method for Rapid Detection of Cyanogenic Bacteria.
1005 *Appl Environ Microbiol* 45:701–702.
1006 98. Kieser T, Bibb MJ, Buttner MJ, Chater KF, Hopwood DA (2000) *Practical*
1007 *Streptomyces Genetics* (John Innes Foundation, Norwich).
1008 99. Caten CE, Jinks JL (1968) Spontaneous variability of single isolates of *Phytophthora*
1009 *infestans*. I. Cultural variation. *Can J Bot* 46:329–348.
1010 100. Zimin AV, et al. (2013) The MaSuRCA genome assembler. *Bioinformatics* 29:2669–
1011 2677.
1012 101. Bankevich A, et al. (2012) SPAdes: a new genome assembly algorithm and its
1013 applications to single-cell sequencing. *J Comput Biol* 19:455–477.
1014 102. Seemann T (2014) Prokka: rapid prokaryotic genome annotation. *Bioinformatics*
1015 30:2068–2069.
1016 103. Hyatt D, et al. (2010) Prodigal: prokaryotic gene recognition and translation initiation
1017 site identification. *BMC Bioinformatics* 11:119.
1018 104. Winsor GL, et al. (2011) *Pseudomonas* Genome Database: improved comparative
1019 analysis and population genomics capability for *Pseudomonas* genomes. *Nucleic*
1020 *Acids Res* 39:D596–D600.
1021 105. Edgar RC (2004) MUSCLE: multiple sequence alignment with high accuracy and high
1022 throughput. *Nucleic Acids Res* 32:1792–1797.
1023 106. Price MN, Dehal PS, Arkin AP (2009) FastTree: computing large minimum evolution
1024 trees with profiles instead of a distance matrix. *Mol Biol Evol* 26:1641–1650.
1025 107. Miller MA, et al. (2015) A RESTful API for Access to Phylogenetic Tools via the
1026 CIPRES Science Gateway. *Evol Bioinform Online* 11:43–48.
1027 108. Letunic I, Bork P (2016) Interactive tree of life (iTOL) v3: an online tool for the display
1028 and annotation of phylogenetic and other trees. *Nucleic Acids Res* 44:W242–W245.
1029 109. Campilongo R, et al. (2017) One ligand, two regulators and three binding sites: How
1030 KDPG controls primary carbon metabolism in *Pseudomonas*. *PLOS Genet*
1031 13:e1006839.

1032 110. Scott TA, Heine D, Qin Z, Wilkinson B (2017) An L-threonine transaldolase is required
1033 for L-threo-β-hydroxy-α-amino acid assembly during obafluorin biosynthesis. *Nat*
1034 *Commun* 8:15935.